CALIFORNIA POLYTECHNIC STATE UNIVERSITY
SAN LUIS OBISPO, CALIFORNIA 93407

Evaluation of Dual Flow Thrust Vector Nozzles with Exhaust Stream Impingement

Final Technical Report 10/90-7/91
NASA-AMES Grant Number NCC 2-686

Dr. Thomas W. Carpenter, Principle Investigator & Professor

The graduate student Don Backlund did not complete his thesis regarding vectored nozzles. Ken Larsen who I was able to parially fund completed his thesis and research. He photographed the shock phenomena using a Schlieren technique and provided an analysis of underexpanded flow for both vectored and non-vectored nozzles. His thesis is included as the final report for NASA-AMES Grant Number NCC 2-686.

A Study of Shock Wave Structure in Underexpanded Jets Exhausting Into Still Air

A Thesis

Presented to the Faculty of

California Polytechnic State University

in Partial Fulfillment

of the Requirements for a Degree of

Masters of Science in Mechanical Engineering

by

Kenneth Michael Larsen

September 1991

ABSTRACT

A STUDY OF THE SHOCK WAVE STRUCTURE IN UNDEREXPANDED JETS EXHAUSTING INTO STILL AIR

Kenneth Michael Larsen
September 1991

The main objective of this project was to predict the expansion wave/oblique shock wave structure in an underexpanded jet expanding from a convergent nozzle. The shock structure was predicted by combining the calculated curvature of the free pressure boundary with principles and governing equations relating to oblique shock wave and expansion wave interaction. The procedure was then continued until the shock pattern repeated itself. A mathematical model was then formulated and written in Fortran to calculate the oblique shock/expansion wave structure within the jet.

In order to study shock waves in expanding jets, Schlieren photography, a form of flow visualization, was employed. Thirty-six Schlieren photographs of jets from both a straight and 15° nozzle were taken. An iterative procedure was developed to calculate the shock structure within the jet and predict the non-dimensional values of Prandtl primary wavelength (w/r_n), distance to Mach Disc (L_d) and Mach Disc radius (r_d). These values were then compared to measurements taken from Schlieren photographs and experimental results published by NASA in Refs(3) and (13).

The results of the method discussed above agreed closely to measurements from Schlieren photographs and data from Refs(3) and (13). This method provides excellent results for pressure ratios below that at which a Mach Disc first forms. Calculated values of non-dimensional distance to the Mach Disc (L_d) agreed closely to values measured from Schlieren photographs and published data. The calculated values of non-dimensional Mach Disc radius (r_d), however, deviated from published data by as much as 25% at certain pressure ratios.

Table of Contents

List of Figures

List of Tables

Nomenclature

A_n	Nozzle exit area
A_t	Reduced throat area
C_d	Discharge coefficient
C_f	Thrust coefficient
C_p	Specific heat at constant pressure
α	Initial flow turning angle at nozzle exit
β	Angle between flow direction and oblique shock wave angle on the other side of the shock wave
γ	Specific heat ratio
δ	Flow turning angle
δ^*	Boundary layer displacement thickness
ε	Oblique shock wave angle
μ	Mach wave angle with respect to flow direction
ν	Prandtl-Meyer angle
ν_o	Kinematic viscosity
ρ	Static density
Γ	Function of γ
b	$\frac{\gamma + 1}{\gamma - 1}$ Constant in Prandtl-Meyer expansion theory
p_o	Ambient pressure
p_j	Nozzle static pressure
P	Total pressure
P_n/p_o	Nozzle total to ambient pressure ratio
p_j/p_o	Nozzle static pressure ratio
M	Mach number

M_j	Nozzle exit Mach number (M_j = 1.0) for choked convergent nozzle
r	Vertical coordinate
r_d	Non-dimensional Mach Disc radius
r_n	Nozzle radius (0.2275 inches)
r/r_n	Non-dimensional vertical coordinate
x	Horizontal coordinate
x/r_n	Non-dimensional horizontal coordinate
L_d	Non-dimensional distance from nozzle to Mach Disc
w	Prandtl primary wavelength
w/r_n	Non-dimensional Prandtl primary wavelength
m	Mass flow rate
R	Ideal gas law constant (53.331 ft-lbf/lbmR for air)
t	Static temperature
T	Total temperature
F_z	Nozzle thrust in the vertical direction (lbf) determined experimentally
F_{net}	Ideal thrust assuming isentropic flow
I_{sp}	Specific impulse (lbf/lbm s)
h	Specific enthalpy (Btu/lbm)
H	Total enthalpy
V_t	Nozzle throat velocity
g	Gravitational constant (32.2 lbm ft/lbf s^2)
B	Body force

CHAPTER 1

Review of Literature

Jet Structure

When a gas exhausts from a nozzle into still air it will undergo an expansion or compression depending on the nozzle exit static pressure to ambient pressure ratio (p_j/p_o). If this ratio is greater than one, the nozzle is underexpanded, and if the ratio is less than one, it is overexpanded Ref(1). In the underexpanded case the jet exhausting into still air will expand in order to equalize with ambient pressure. Expansion or compression at the nozzle exit can occur whether the nozzle contour is convergent (known as sonic) or convergent-divergent (known as supersonic). Expansion or compression of an exhaust jet can be accomplished for given nozzle inlet conditions by variation of the nozzle back pressure.

In this project, a convergent nozzle mounted on a six component thrust stand was supplied by compressed air and exhausted into ambient air. Schlieren photographs were taken at various inlet pressures for the cases of a straight and 15° convergent nozzle. In each case photographed, the nozzle was underexpanded. In addition, the nozzle total pressure to ambient pressure ratios exceeded the critical pressure ratio in all cases photographed and consequently the flow was choked (M = 1.0) Ref(2).

The critical pressure ratio (P_n/p_j) for air behaving as an ideal gas with a constant specific heat ratio of 1.4 is 0.52828 Ref(2). Therefore, the minimum nozzle total pressure required to choke the flow for an ambient air pressure of 14.7 psia is 27.8 psia. It is of interest to note that the shock diamond structure is first observed in Schlieren Photograph No. 22 and is provided in Figure 1. The corresponding nozzle total pressure in this

photograph is 31.7 psia. Since shock waves cannot form in subsonic flow, the nozzle must be choked before shocks can appear in the jet.

As the jet expands from the nozzle, a constant pressure boundary forms Ref(3). This boundary indicates the region in which the static pressure of the jet equals ambient pressure. The slope of this boundary is a maximum at the nozzle exit (where expansion is greatest) and gradually diminishes until the jet stops expanding and compression begins Ref(4). The result is a parabolic-shaped boundary with a point of inflection where compression begins.

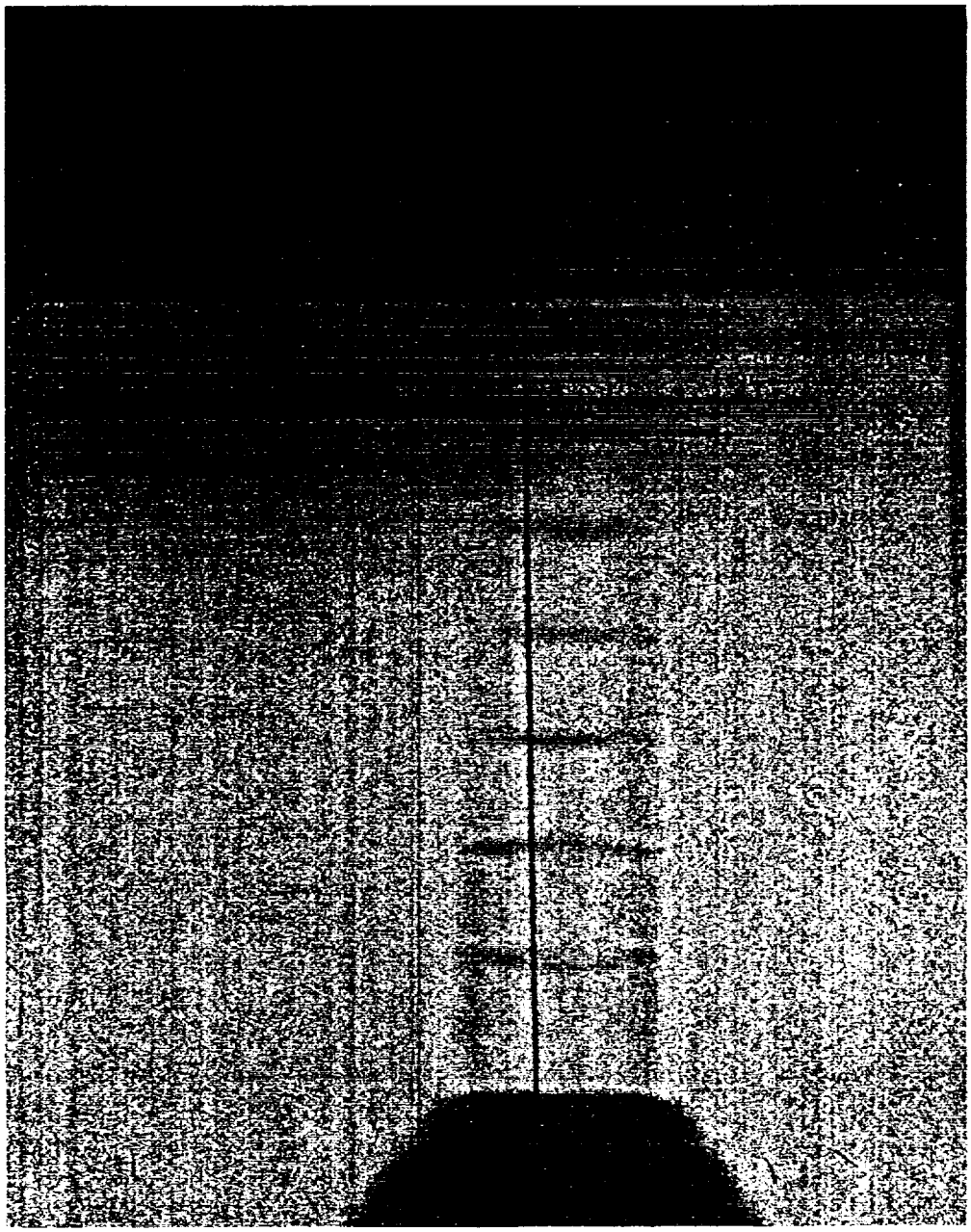

Figure 1. Formation of Shock Diamond

Figure 2 illustrates the theoretical structure of the jet expanding from an underexpanded convergent nozzle into still air Ref(1), (31) and (43).

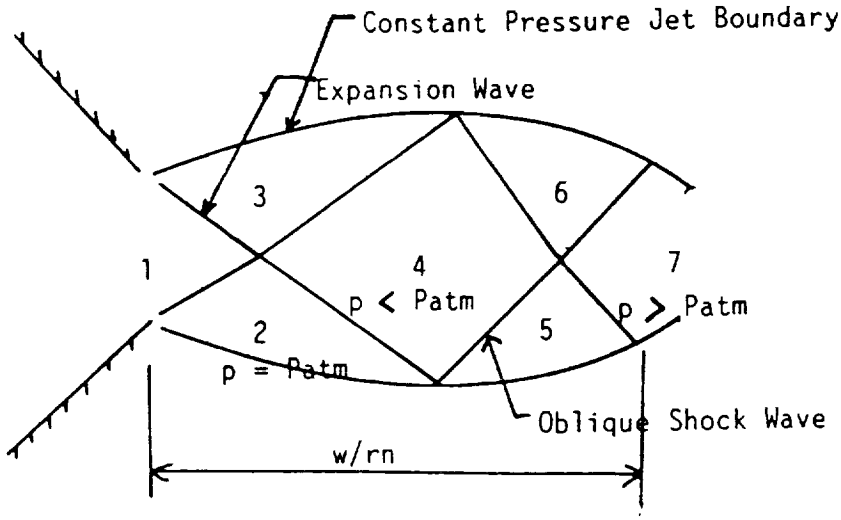

Figure 2. Jet Structure of an Axisymmetric Jet Exhausting Into Still Air

Since the flow is choked, the Mach number at the exit of the nozzle (Region 1) is 1.0. At this point the flow is assumed to expand to atmospheric pressure isentropically via Prandtl-Meyer expansion Ref(3). As the flow expands from Region 1 to 2, it accelerates to supersonic speed and its static pressure decreases to atmospheric pressure. In addition, static temperature and density decrease as the flow expands.

The expansion from Region 1 to 2 is modeled as a discrete expansion wave. In actuality, there is an expansion fan consisting of an infinite number of Mach waves Ref(3). This discrete expansion wave is the average of the initial and final Mach waves. The calculation of the angle of the discrete expansion wave with respect to the flow axis is shown in Appendix A. From symmetry, the angle of the discrete expansion waves from the upper and lower edges of the nozzle are equal. Between Regions 1 and 4, the discrete

expansion waves intersect and reflect at the centerline of the flow. Expansion waves of equal strength reflect in the same manner as reflection from a solid surface. Therefore, as the flow passes from Region 2 to 4, it encounters another expansion wave. As a result, its static pressure decreases to a value less than atmospheric pressure.

The expansion waves then reflect from the free pressure boundary. From the principles of expansion waves and oblique shock waves (Appendix A), expansion waves reflect from free pressure boundaries as oblique shock waves. Therefore, from Region 4 to 5 in Figure 2, the flow passes through a reflected oblique shock wave. Since the flow passes through an oblique shock wave its static pressure increases to atmospheric pressure in Region 5 in order to equalize with the free pressure boundary. The flow Mach number decreases and static pressure, temperature and density increase as the flow passes through an oblique shock wave Ref(2). The flow structure on the upper and lower sections of the jet in Figure 2 are assumed to be symmetric.

The oblique shock waves then intersect at the centerline between Regions 4 and 7. Oblique shock waves of equal strength reflect in the same manner as a reflection from a solid surface. Therefore, as the flow passes from Region 5 to 7, it encounters another oblique shock wave. The static pressure in Region 7 is therefore greater than atmospheric pressure. Finally, the reflected oblique shock waves meet the free pressure boundary and reflect as expansion waves Ref(2).

The oblique shock waves in Region 7 reflect from the constant pressure jet boundary as expansion waves. These expansion waves would then intersect and reflect at the centerline in an identical fashion to the flow from Region 1 to 4. The flow pattern beyond Region 7 therefore repeats itself.

The point at which the jet shock pattern repeats itself is known at the Prandtl primary wavelength (w/r_n) and the repeating shock diamond structure was first detected by L. Prandtl using Schlieren photographs Ref(5). The shock structure discussed and illustrated in Figure 2 occurs at pressure ratios below that at which a Mach Disc first appears. The Mach Disc is a normal shock wave that appears between Regions 4 and 7. The Prandtl primary wavelength is an important aspect of the study of axisymmetric free jets. This point is readily visible in all Schlieren photographs. The length (w/r_n) is a non-dimensional distance and is easily measured from Schlieren photographs. Results of measurements of Prandtl primary wavelength measured from photographs taken in this project are compared with results from other references in the results section of the report.

Constant Pressure Jet Boundary

The first step in the calculation of the jet structure was to determine the contour of the constant pressure jet boundary at various nozzle pressures. The structure of the expansion/oblique shock waves within the jet was then calculated using the governing equations for oblique shocks, expansion waves, and normal shock waves in conjunction with the jet boundary contour. The jet boundary contour was provided in the form of a 3rd order polynomial.

The constant pressure jet boundary contour was solved by using the method of characteristics. Analytical work was conducted by D. C. Pack in 1947 Ref(6) and compared with Schlieren photographs in 1959 by Love, Grisby, Lee and Woodling Ref(3). L. Prandtl first used Schlieren photographs to study jets exhausting form a convergent nozzle or orifice and was discussed in Ref(5). Love and Grisby used the method of characteristics to determine the contour of the constant pressure jet boundary. In this

report, an alternative method of predicting the constant pressure jet boundary contour proposed by Adamson and Nicholls Ref(4) was used.

The first step in the solution of the jet boundary was to determine the initial flow angle of the jet at the nozzle exit. If the air was assumed to undergo a Prandtl-Meyer expansion at the nozzle exit then the initial flow angle was given as follows Ref(2).

$$\alpha = \nu_2 = -(b)^{1/2} \tan^{-1} [(M_2^2 - 1.0)/b]^{1/2} + \tan^{-1} (M_2^2 - 1.0)^{1/2} \qquad \text{Eqn(1)}$$

where: $$b = \frac{\gamma + 1}{\gamma - 1}$$

The derivation of Equation 1 is provided in Appendix A. As discussed earlier, this was the maximum slope of the constant pressure jet boundary.

The flow angle or tangent of the jet boundary curve at any point is simply the difference between the initial flow angle (α) and the Prandtl-Meyer angle (δ) at that location. The slope of jet boundary at any point can therefore be put in terms of the vertical and horizontal coordinators r and x as follows.

$$\tan (\alpha - \delta) = dr/dx$$

Separating variables, integrating and putting r and x into non-dimensional form r/r_n and x/r_n where r_n is the nozzle radius.

$$x/r_n = \int_1^{r/r_n} d(r/r_n) / \tan(\alpha - \delta) \qquad \text{Eqn(2)}$$

The integration of Equation 2 can be solved numerically using either the Newton-Cotes, Simpson's 1/3 or Simpson's 3/8 methods Ref(11).

Adamson's paper Ref(4) suggested that the integration method should give good results for relatively low pressure ratios compared with the method of characteristics. The results of jet boundary calculations using the Adamson-Nicholls method at pressure ratios of 2, 10, and 20 are compared with results from Love, Grisby Ref(3) in Figure 3. This method provides an accurate prediction of the jet boundary contour at low pressure ratios and departs from the method of characteristics solution as the pressure ratio increases. More importantly, the calculated boundary contour closely approximates the actual boundary measured from Schlieren photographs. Since the pressure ratios encountered in this project range from 1.1 to 3.2, the Adamson-Nicholls method of Ref(3) was sufficient. A convenient feature of the use of non-dimensional variables was that different experiments could be compared, independent of the nozzle dimensions used in each experiment.

Oblique/Expansion Wave Structure Within a Jet

The next area of interest in the study of jets exhausting into still air was the formation and interaction of expansion and shock waves in the flow. Previous work in this area used the method of characteristics to predict the jet structure Ref(3). However, the method of characteristics was limited to those jet structures without Mach Discs. In this report, the prediction of the jet structure was simplified when reflection and intersection of discrete expansion waves, normal and oblique shock waves in quasi-one-dimensional flow were considered. The principles of expansion and oblique shock wave interaction are presented in Appendix A.

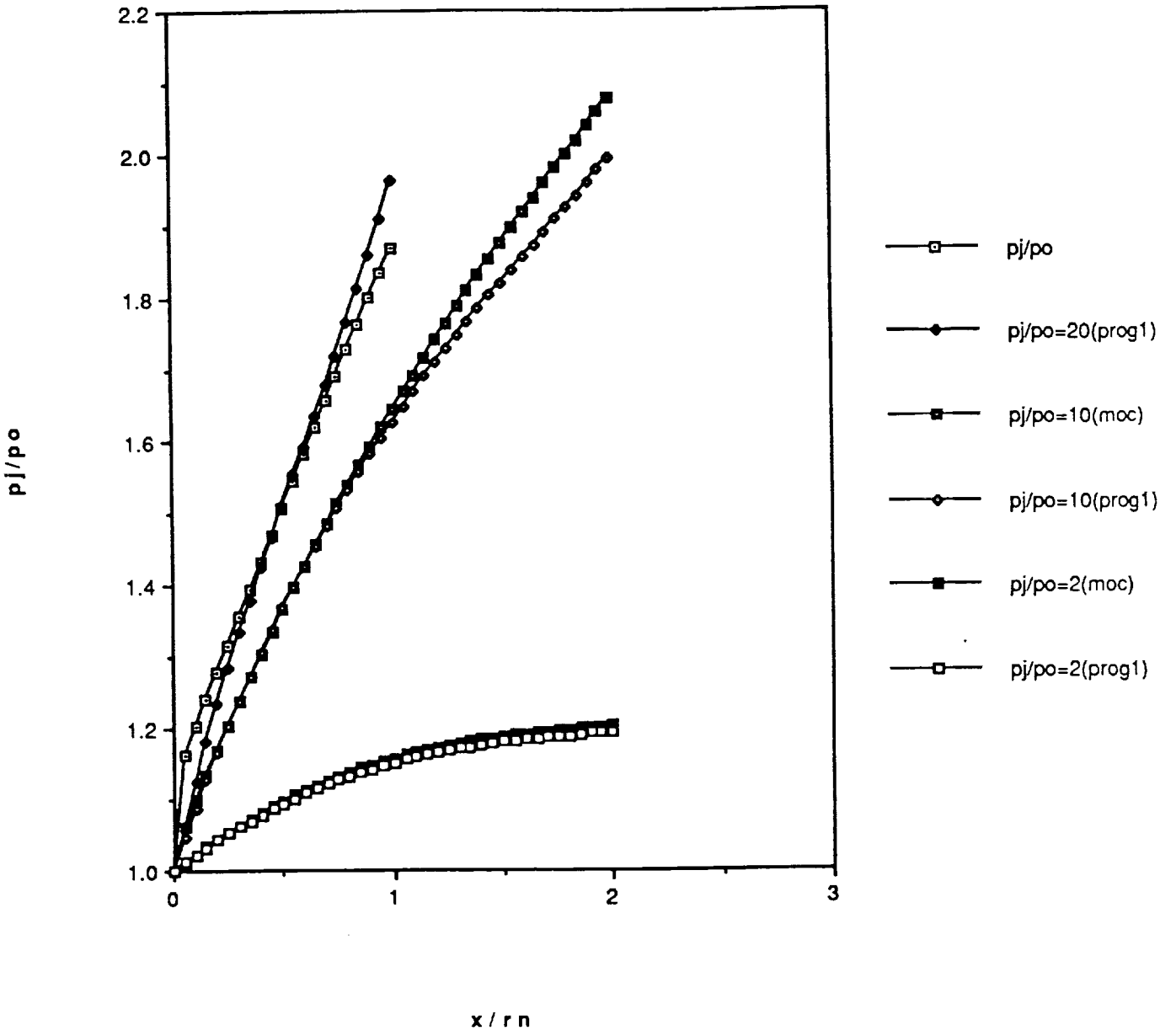

Figure 3. Comparison of Method of Characteristics Solution with Jet Boundary Program

The general structure of the axisymmetric jet has been described. With this general structure known, in addition to the nozzle inlet conditions, the governing equations of expansion waves and oblique shock waves were used to determine the jet structure as a function of inlet pressure. That is, with nozzle inlet conditions known, the governing equations of oblique shock waves and Prandtl-Meyer expansion were used to determine the expansion wave angles (μ), the oblique shock wave angles (ϵ) and the flow turning angles (δ) throughout the flow structure. With these values known in addition to the curvature of the jet boundary, the jet structure was defined. Consequently, the Prandtl primary wavelength (w/r_n) was calculated for a given nozzle inlet pressure. The exact calculational procedure for predicting the jet structure was provided in Appendix B.

Love, Grisby Ref(3) developed empirical relations (based on measurements from Schlieren photographs) for predicting the Prandtl primary wavelength for the case of no Mach Disc present and for the presence of a Mach Disc. The two equations are as follows.

No Mach Disc present ($p_j/p_o < 2.0$):

$$w/r_n = 3.1[\, Mj^2\, (p_j/p_o) - 1\,]^{1/2}$$

Mach Disc present ($p_j/p_o > 2.0$):

$$w/r_n = 3.04(p_j/p_o)^{0.437} + 3.1\, [\, (2\, M_j^2 - 1)^{1/2} - 1\,] - (0.55)\, \beta_j + 0.5\, \{\, (1/1.55)\, [\, (\, p_j/p_o - 2\,)\, \beta_j\,]^{1/2} - 1\, \}$$

Where: w/r_n = Non-dimensional Prandtl primary wavelength

M_j = Mach number at nozzle exit (M_j = 1.0 in this case)

$\beta_j = (M_j - 1.0)^{1/2} = 0.0$ (for $M_j = 1.0$)

For the case of a convergent nozzle (Mj = 1.0) these equations simplify as follows.

No Mach Disc present:

$$w/r_n = 3.1 \left[(p_j/p_o) - 1 \right]^{1/2} \qquad \text{Eqn(3)}$$

Mach Disc present:

$$w/r_n = 3.04(p_j/p_o)^{0.437} - 0.5 \qquad \text{Eqn(4)}$$

Formation of the Mach Disc

The next step in the study of jet structures was to model the Mach Disc phenomenon. The case illustrated in Figure 2 is known as a regular oblique shock wave reflection. In this case, the reflected oblique shock between Regions 5 and 7 is strong enough to straighten out the flow to become parallel to the original flow axis Ref(1). A Mach Disc forms when a regular reflected oblique shock wave from Region 5 to 7 cannot straighten out the flow. At pressure ratios above this point, a Mach Disc becomes visible in Schlieren photographs. This phenomenon of irregular oblique shock wave reflection is known as Mach reflection Ref(7). Figure 4 illustrates the change in shock diamond structure from Region 4 to 7 when a Mach Disc forms.

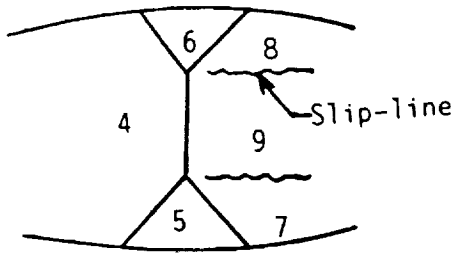

Figure 4. Mach Disc Structure

The Mach Disc forms when the initial oblique shock wave formed between Regions 4 and 5 generates a reflected oblique shock with a corresponding deflection angle greater than the maximum deflection angle (δ_{max}). That is, when the deflection angle corresponding to the Mach number in Region 5 (behind the incident oblique shock) is insufficient to straighten out the flow, a Mach Disc forms Ref(6). The maximum deflection angle associated with an oblique shock wave is given as follows and was derived in Appendix A.

$$\delta_{max} = \frac{r - 1}{2(r)^2} \qquad \text{Where:} \quad r = \frac{\rho_2}{\rho_1} \qquad \text{Eqn(5)}$$

Additional information desired with regards to the Mach Disc is the non-dimensional radius (r_d) and non-dimensional distance to the Mach Disc (L_d). The Mach Disc is modeled as a normal shock wave. In actuality, it has a slight curvature Ref(7). A Mach Disc is a normal shock wave that connects four oblique shock waves. In Figure 4, Regions 4, 5 and 6 coincide with those in Figure 2.

In the case of a Mach Disc another area of interest appears, the region behind the normal shock. From Figure 4, the Mach numbers in Regions 7, 8, and 9 are different.

The only flow property in common between Regions 7, 8, and 9 is the static pressure. Since there is a difference in properties between these regions a discontinuity appears in the form of a slip-line Ref(8). The slip-line is visible in some photographs in Ref(7), however, it does not appear in any photographs taken in this project. Higher resolution photography should visualize the slip-lines.

The next step in the study of Mach Disc formation was to determine the size and location of the Mach Disc. That is, the non-dimensional distance to the Mach Disc (L_d) and the non-dimensional radius (r_d). Analysis involving the method of characteristics was unable to accurately predict the geometry of the Mach Disc. Recall the Love, Grisby empirical relationship for the Prandtl primary wavelength with a Mach Disc present in the jet (Equation 4).

$$w/r_n = 3.04(p_j/p_o)^{0.437} - 0.5$$

If w/r_n is known by actual measurement or by use of Equation 4, then the structure of the Mach Disc can be determined using data calculated with the Jet Boundary and Jet Structure programs. A calculational procedure for predicting the Mach Disc distance and radius as a function of the nozzle pressure was developed and is presented in Chapter 3 and a sample calculation provided in Appendix G.

CHAPTER 2

Method of Experimentation

Principles of Schlieren Photography

An important aspect of this project was the flow visualization of the air discharging from the straight and 15° convergent nozzles. The technique employed was Schlieren photography. The method was first developed by Foucault (1859) and Toepler (1864) Ref(10). L. Prandtl first used Schlieren photography to study the shock wave phenomenon in axisymmetric jets. The basic principle behind Schlieren photography is that certain types of discontinuities or property variations in a transparent media refract light. The result is an image or trace of the discontinuity onto a photographic plate in the form of a shadow. In this case air was exhausted from a convergent nozzle at high pressure into still air. The air undergoes changes in static density, pressure and temperature as it flows out of the nozzle and expands. In addition, expansion waves, normal, and oblique shock waves form in the flow. As light passes through the discontinuity or shock waves, the light is refracted resulting in an image of the shock which can then be photographed.

The primary components of the Schlieren apparatus used in this project and illustrated in Figure 5 are the light source, light slit, two Schlieren mirrors, knife edge and photographic plate (35 mm camera in this case). This variation of Schlieren system is known as the Barnes and Bellinger, or two mirror system Ref(10). The light source used was a Halogen lamp placed at a distance corresponding to the focal length of the first mirror. Each Schlieren mirror has a 48 inch focal length and a 4 inch diameter. The maximum field of view of a photograph is therefore limited to 4 inches. There is a slit located between the light source and first Schlieren mirror. The light slit concentrates the light onto the first Schlieren mirror. The Schlieren mirrors are positioned so that the flow

field is located between them. A knife edge is placed at the focal length of the second mirror. The purpose of the knife edge is to reduce the intensity of the light exposing the photographic surface and create a dark ground condition, Ref(10). The light source, slit, and knife edge are placed parallel to one another.

Schlieren photographs were taken with and without the use of the knife edge. Photographs made without the knife edge gave greater detail of the flow. The photographs presented in Appendix D were made at a wide range of nozzle total pressures. Photographs were also taken using two different techniques of camera arrangement. In the first method, light passes through the knife edge which shines directly onto a 35 mm camera with the lens removed. This method required the use of low ASA film (125) and fast shutter speeds (1/500 to 1/1000 sec). The absence of a knife edge under these circumstances results in severe overexposure of the film regardless of the ASA used. In the second method, the beam of light was reflected from a flat reflective surface and a photograph was taken of the reflection. This method allowed photographs to be taken with or without a knife edge. Unlike the first method, this method required the use of extremely high ASA film (3200) and low shutter speeds (1/4 to 1/8 sec).

The best results were achieved using the second method of camera arrangement. The Schlieren system is conceptually simple and was set up easily. However, the difficulty of Schlieren photography occurred when experimenting with shutter speeds and film type to achieve the best photographic results. In addition, complete darkness in the laboratory is essential to ensure proper film exposure.

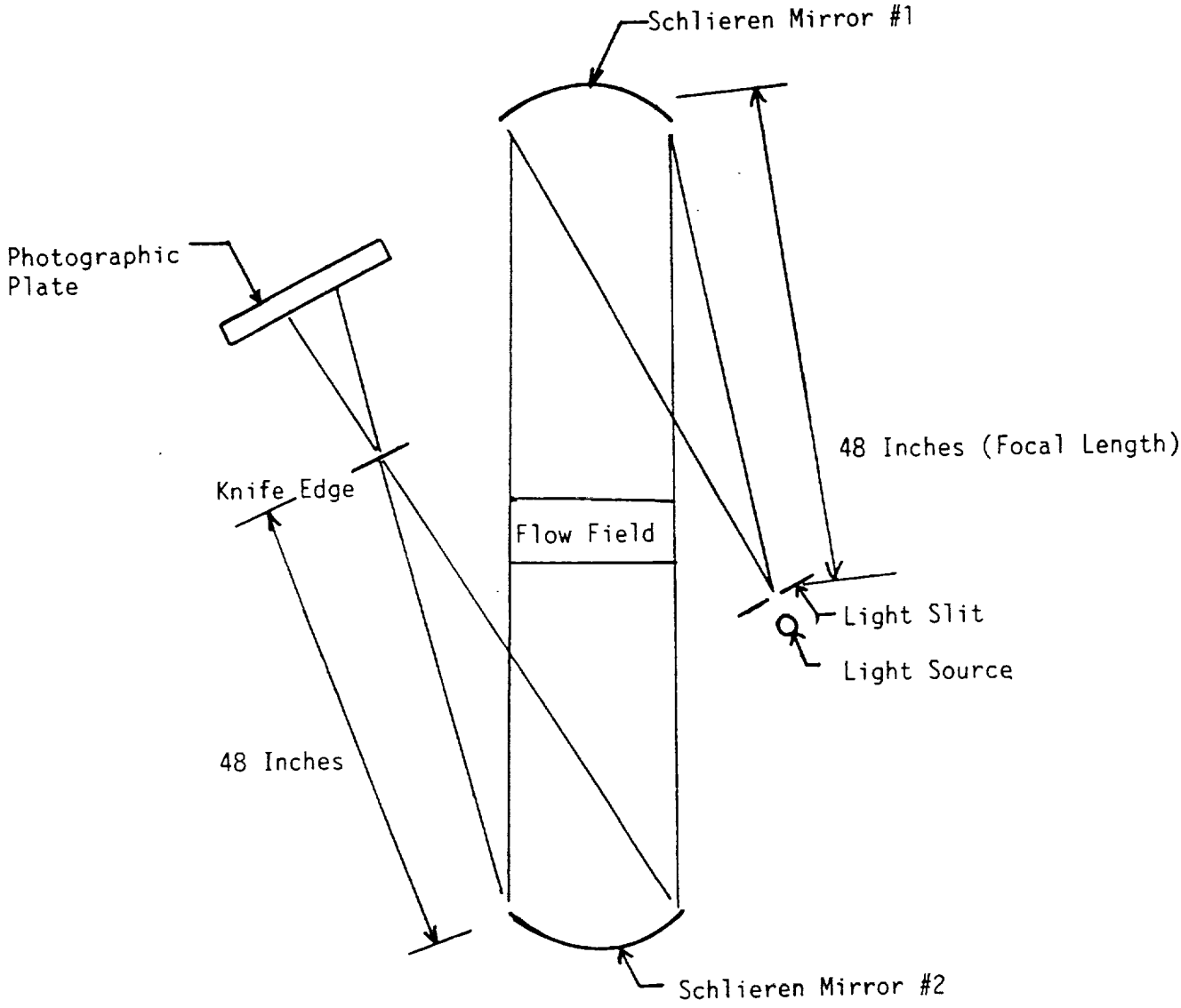

Figure 5. Schlieren System Apparatus

Thrust Stand Data Acquisition

The primary component of the thrust stand assembly are the convergent nozzle (straight and 15°), air inlet plenum, thrust stand, isolation mounts or bellows, load cells for force measurement and pressure transducers. One pressure transducer is located in the inlet plenum and measures static pressure. The second pressure transducer is located just before the nozzle inlet and measures total pressure. There were 6 load cells measuring forces in the x, y, and z directions.

Data from the pressure transducers was sampled by the Fluke Data Acquisition System where the date was displayed and printed. A printout of pressure and force measurements was made for each Schlieren photograph presented and an example is provided in Appendix J. Each printout contains the nozzle inlet total pressure and load cell readings from each of the six component load cells. Additional experimental data that needed to be determined was the system total temperature (storage tank temperature) and barometric reading.

CHAPTER 3

Analytical Analysis

Calculation of Constant Pressure Jet Boundary

Recall that in the Constant Pressure Jet Boundary section of Chapter 1 that the integral representing the jet boundary defined by Equation 2 was as follows:

$$x/r_n = \int_1^{r/r_n} d(r/r_n) / \tan(\alpha - \delta) \qquad \text{Eqn(2)}$$

Where

δ = Difference in Prandtl-Meyer angles at any location along the jet boundary.

$$\delta = \nu_2 - \nu_1 = -(b)^{1/2} \{\tan^{-1}[(M_2^2 - 1.0)/b]^{1/2} - \tan^{-1}[(M_1^2 - 1.0)/b]^{1/2}\} + [\tan^{-1}(M_2^2 - 1.0)^{1/2} - \tan^{-1}(M_1^2 - 1.0)^{1/2}]$$

α = Initial jet turning angle defined by Equation 1. This value remained constant throughout the calculation and was a function only of the nozzle pressure (P_n).

$$\alpha = \nu_2 = -(b)^{1/2} \tan^{-1}[(M_2^2 - 1.0)/b]^{1/2} + \tan^{-1}(M_2^2 - 1.0)^{1/2} \qquad \text{Eqn(1)}$$

$$b = \frac{\gamma + 1}{\gamma - 1}$$

The integral in Equation 2 can be numerically calculated. The Simpson's 3/8 rule of integration was defined as follows Ref(11).

$$x = (3/8)\, H\, (F_o + 3F_a + 3F_b + 2F_c + 3F_d + 3F_e + 2F_f + 3F_g + 3F_h + F_i)$$

H = Amount that the r coordinate is incremented (variable).

x = Distance along the flow axis.

The numerical procedure is outlined as follows.

Evaluate function of F_o:

The value of F_o was the value of the function within the integral sign in Equation 2.

$$F_o = 1/\tan(\alpha - \delta_o)$$

The value δ_o was the difference in Prandtl-Meyer angles at the start of the integration. In this case it was the nozzle exit so ($\delta_o = 0$). F_o then becomes.

$$F_o = 1/\tan(\alpha)$$

Evaluate function values F_a through F_i:

1. Select a value for H and increment r by H.

$$r_a = r_n + H$$

2. Evaluate the critical area ratio Ref(2) at point a.

$$(A/A^*)_a = (r_a/r_n)^2 \ (A/A^*)_E$$

A^* = Nozzle exit area (0.1625 in^2)

r_n = Nozzle radius (0.2275 in)

$(A/A^*)_E$ = Critical area ratio associated with the Mach number at the end of the Prandtl-Meyer expansion at the nozzle exit.

Solve for $(A/A^*)_E$

$$(A/A^*)_E = \frac{1}{M_E^2} \left[\frac{2}{\gamma+1} \left(1 + \frac{\gamma - 1}{2} M_E^2 \right) \right]^{\frac{\gamma+1}{2(\gamma-1)}}$$

Where M_E is the Mach number after the initial Prandtl-Meyer expansion from the nozzle and was defined by Equation 10a in Appendix A. Substitute r_a, r_n and $(A/A^*)_E$ into the above equation and solve for $(A/A^*)_a$.

3. Solve for Mach number at location a (M_a) implicitly from the following equation.

$$(A/A^*)_a = \frac{1}{M_a^2}\left[\frac{2}{\gamma+1}\left(1+\frac{\gamma-1}{2}M_a^2\right)\right]^{\frac{\gamma+1}{2(\gamma-1)}}$$

4. Solve for δ_a by substituting M_a and M_E into the expression for δ defined above.

5. Solve for the function value at location a (F_a).

   $F_a = 1/\tan(\alpha - \delta_a)$

6. Increment r_a by H

   $r_b = r_a + H$

7. Return to Step 2 and solve for $(A/A^*)_b$

   Where: $(A/A^*)_b = (r_b/r_n)^2 (A/A^*)_E$

8. Calculate F_b.

   $F_b = 1/\tan(\alpha - \delta_b)$

9. Repeat procedure until F_i is calculated.

10. Substitute values of F_o through F_i into the Simpson's 3/8 Rule equation and solve for x. Make values of r and x non-dimensional by dividing by the nozzle radius r_n and store values. This completes the integration for one data point.

11. Set $F_o = F_i$ and return to Step 1 to begin integration again.

12. Repeat the procedure until the desired number of jet boundary data points are generated.

The above procedure for calculating the jet boundary was programmed into the Jet Boundary Fortran program presented in Appendix F. The program generated values of r/r_n and x/r_n along the jet boundary in accordance with the Adamson-Nicholls integration technique of Ref(4). The only data that the user must input into the program was the nozzle total pressure (P_n). Values of r/r_n and x/r_n from the Jet Boundary program were

then put into a curve fitting program in order to calculate a 3rd order polynomial representing the jet boundary. This process was completed for pressures corresponding to the Schlieren photographs. The resulting jet boundary contours are presented in Appendix E.

Calculation of Jet Structure (No Mach Disc Present)

The general jet structure illustrated in Figure 2 and discussed in the Jet Structure section of Chapter 1 represented the case of no Mach Disc present in the flow. For given nozzle inlet conditions, the discrete expansion wave angles (μ), oblique shock wave angles (ϵ) and flow turning angles (δ) throughout the flow can be calculated using the governing equations of oblique shock waves and Prandtl-Meyer expansion. The jet boundary contour was calculated using the Adamson-Nicholls integration method and a 3rd order polynomial representing the curve was generated. With the expansion/oblique shock wave angles known in addition to the boundary contour, the geometry of the jet structure can be determined. Figure 2 is repeated at this time for convenience.

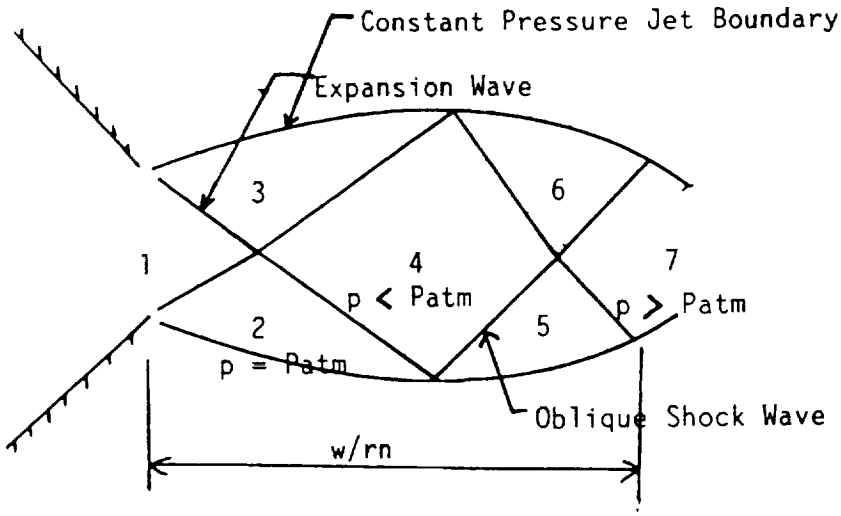

Figure 2. Jet Structure of an Axisymmetric Jet Exhausting Into Still Air

The calculational procedure for determining the jet structure and ultimately the Prandtl primary wavelength (w/r_n) for the case of no Mach Disc present in the flow is presented below.

1. Calculate the Mach number in Region 2 with nozzle total pressure (P_n) known. Substitute into Equation 10a of Appendix A.

2. Solve for the initial flow turning angle (α) using Equation 1.

3. Solve for the angle of the discrete expansion wave (average Mach wave angle μ_{ave}). This was the angle the discrete expansion wave at the nozzle exit makes with respect to the flow axis.

4. Solve for the discrete expansion wave angle (with respect to the flow axis) from Region 2 to 4. This was the expansion wave reflected at the flow centerline.

5. Introduce the jet boundary contour 3rd order polynomial and solve for non-dimensional distance ($x_1 + x_2$).

6. Using the governing equations of oblique shock waves, the geometry of the shock structure and the jet boundary contour, solve for non-dimensional distance ($x_3 + x_4$).

7. Determine the Prandtl primary wavelength w/r_n by adding the non-dimensional distances x_1 through x_4.

$$w/r_n = x_1 + x_2 + x_3 + x_4$$

This calculational procedure was carried out in the sample calculation provided in Appendix B. The Jet Structure program was written to calculate the Prandtl primary wavelength (w/r_n). The program requires the user to input nozzle total pressure (P_n), total temperature (T_n) and the four coefficients associated with the jet boundary 3rd order polynomial. The program is presented in Appendix G.

Calculation of Jet Structure (Mach Disc Present)

Figure 4 is repeated at this time for convenience.

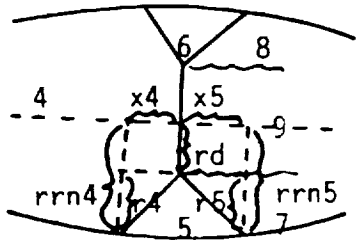

Figure 4. Mach Disc Structure

The procedure for calculating the non-dimensional distance to the Mach Disc (L_d) and Mach Disc radius (r_d) is as follows.

1. Solve for flow properties in Regions 1 through 6 in the same manner as the case of no Mach Disc present.

2. Solve for the non-dimensional distances x_1, x_2 and x_3 in the same manner as in the case of no Mach Disc present.

   Define: $x/r_n = x_1 + x_2 + x_3$

3. Use the governing equations of oblique shock waves, solve for the oblique shock wave angle ε_{45} and flow turning angle δ_{45} for the initial reflected oblique shock from Region 4 to 5.

4. Using the governing equations of normal shock waves, solve for the flow properties in Region 9.

5. Set the static pressures in Regions 7, 8, and 9 equal.

6. Solve for the flow properties in Regions 7, 8, and 9 and the oblique shock wave angle ε_{57} and the flow turning angle δ_{57} (reflected oblique shock).

7. Verify that δ_{57} is less than the δ_{max} corresponding to the Mach number in Region 5 using Equation 5.

8. Determine the value of the Prandtl primary wavelength w/r_n from either Equation 4 or measurement from a Schlieren photograph. Use w/r_n, the value of x/r_n determined in Step 2, the jet contour and the geometry of the Mach Disc structure in Figure 4 to calculate values of r_d and L_d.

Where r_d = Mach Disc radius
L_d = Distance to Mach Disc

9. Compare calculated values of L_d and r_d with those determined from curve fitting NASA graphical data from Ref(10). These equations were determined as follows.

$$r_d = -0.948 + 0.673\,(p_j/p_o) - 0.086\,(p_j/p_o)^2 + 0.0043\,(p_j/p_o)^3$$

$$L_d = 0.055 + 1.396\,(p_j/p_o) - 0.198\,(p_j/p_o)^2 + 0.013\,(p_j/p_o)^3$$

A sample calculation of the above procedure was conducted for the case of $P_n = 89.0$ psia and is presented in Appendix C. The Jet Structure Fortran program was written to carry out this calculation and is presented in Appendix G.

CHAPTER 4

Experimental Results

Schlieren Photographs

Thirty-six Schlieren photographs were taken of the straight and 15° convergent nozzles. These photographs are presented in Appendix D. Figure 6 (Photo No. 29) is an example of a Schlieren photograph of the straight nozzle at a pressure ratio at which there is no Mach Disc present in the flow. Figure 7 (Photo No. 30) is also a Schlieren photograph also of a straight nozzle. However, in this photograph a Mach Disc is present in the flow.

Values of Prandtl primary wavelength (w/r_n) measured from Schlieren photographs taken in this project for the straight and 15° nozzles are provided in Table 1. In each case the pressure ratio is below that at which a Mach Disc first forms in the flow. These values are compared with values predicted by the NASA empirical relation Equation 3 from Ref(3).

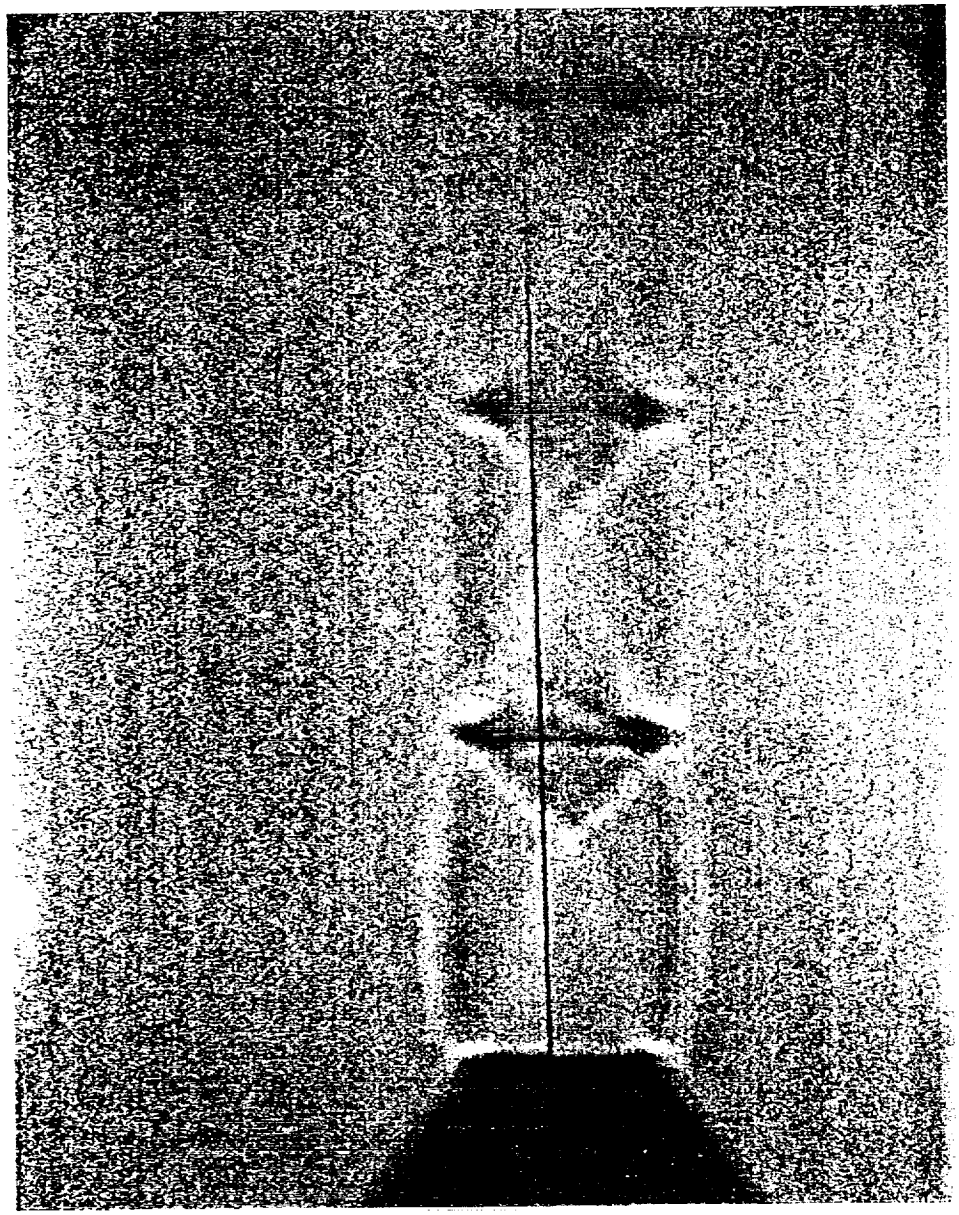

Figure 6. Schlieren Photo No. 29

P_n = 75.6 psia

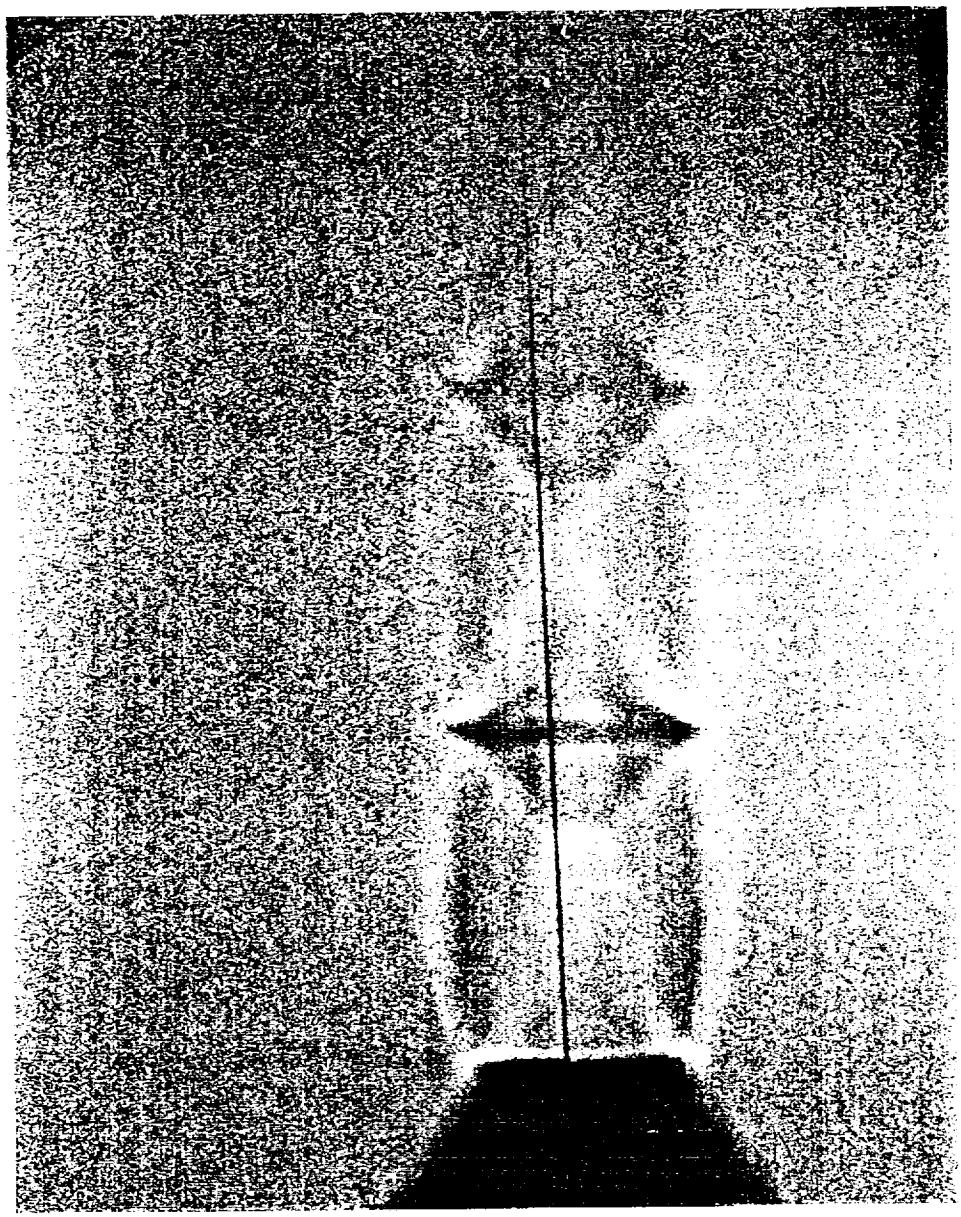

Figure 7. Schlieren Photo No. 30

P_n = 88.6 psia

Table 1
Comparison of Prandtl Primary Wavelength Data (No Mach Disc)

Photo No.	P_n (psia)	p_j/p_o	w/r_n (photo)	w/r_n Eqn(3)
15° Nozzle				
13	35.4	1.27	1.62	1.63
14	42.1	1.51	2.10	2.21
15	52.0	1.87	3.00	2.88
16	58.4	2.10	3.29	3.25
17	65.9	2.37	3.50	3.62
18	68.2	2.45	3.88	3.73
Straight Nozzle				
23	35.5	1.20	1.62	1.60
24	42.0	1.51	2.14	2.21
25	51.7	1.86	2.68	2.87
26	58.3	2.10	3.33	3.24
27	66.0	2.37	3.71	3.63
28	67.8	2.44	3.71	3.71
29	75.7	2.72	4.00	4.07

In Table 1, measurements from Schlieren photographs agree very closely with those determined by NASA in Ref(3).

Recall that in the Constant Pressure Jet Boundary section of Chapter 1, the first step in the solution of the jet boundary was to determine the initial flow angle (α) of the jet. In Appendix A, the procedure for calculating this angle was presented. The following table compares the calculated values of initial flow angle with those predicted in Ref(3).

Table 2
Initial Jet Flow Angle

Photo No.	P_n (psia)	p_j/p_o	α°	α Ref(3)
1	32.4	1.164	1.85	---
2	35.3	1.268	3.38	---
3	41.9	1.520	6.94	6.9
4	51.8	1.854	10.99	11.1
5	57.8	2.080	13.33	13.4
6	66.2	2.379	16.01	16.0
7	67.5	2.440	16.52	16.4
8	75.2	2.731	18.71	18.8
9	79.8	2.875	19.69	19.8
10	88.8	3.191	21.67	21.6
11	96.5	3.468	23.21	23.1

Jet Structure Calculation (No Mach Disc Present)

In the sample calculation provided in Appendix B the pressure ratio was (p_j/p_o = 2.0). The Prandtl primary wavelength (w/r_n) was calculated as 3.16. Substituting p_j/p_o into Equation 3, the value of NASA's predicted value of w/r_n was 3.1. The two values are within 2%. Values of calculated Prandtl primary wavelength (w/r_n) predicted by NASA Equation 3 and values measured from Schlieren photographs in this project are compared with those predicted using the Jet Boundary and Jet Structure programs. Results are summarized in the following table.

Table 3
Comparison of Prandtl Primary Wavelength Data With Jet Strucutre Program Results (No Mach Disc)

Photo No.	P_n(total)	p_j/p_o	w/r_n(Program)	w/r_n(NASA)	%Dev	w/r_n(photo)
24	40.0	1.44	2.11	2.06	2.4	2.13
---	45.0	1.62	2.47	2.44	1.9	---
25	51.7	1.86	2.95	2.87	2.7	2.90
---	55.6	2.00	3.16	3.10	1.9	---
26	58.3	2.10	3.29	3.24	1.5	3.40
27	66.0	2.37	3.73	3.63	2.7	3.49
---	70.0	2.52	3.72	3.82	2.6	---

The Jet Structure program predicts Prandtl primary wavelength (w/r_n) values quite close to those predicted by NASA Equation 3 and values obtained from Schlieren photograph measurements.

Calculation of Mach Disc Formation Pressure

In the sample calculation in Appendix B, p_j/p_o was 2.0, corresponding to a nozzle total pressure of 55.65 psia. The value for $(\delta)_{max}$ in Region 5 to 7 was calculated as 14.5° which was greater than the (δ) required to straighten out the flow (12.5°). Therefore, no Mach Disc was formed at this pressure ratio.

A piece of information that is desired is the total pressure or static pressure ratio at which $(\delta)_{max}$ is first exceeded in Region 5 to 7 (reflected oblique shock) and consequently the pressure at which a Mach Disc should form. This can be calculated using the Jet Boundary and Jet Structure programs. The following calculational procedure is presented.

1. Increment the nozzle total pressure above 55.65 psia and run the Jet Boundary program to calculate the constant pressure boundary.

2. Insert jet boundary data into a curve fitting program to generate a 3rd order polynomial representing the jet boundary.

3. Input above data into the Jet Structure program to see if $(\delta)_{max}$ is exceeded. If not, increment the total pressure and return to Step 1.

The above procedure was completed and the nozzle total pressure at which the Mach Disc should first appear was calculated as 72.5 psia. This prediction was substantiated by experimental work conducted by Addy in Ref(12) and data provided by NASA in Ref(13). Addy's paper predicts that the Mach Disc will first form at a nozzle

total pressure ratio (P_n/p_o) of 5.0 or (P_n = 73.5 psia). In Schlieren Photo No. 28 (P_n = 68.4 psia) there is no indication of a Mach Disc, in Photo No. 29 (P_n = 75.6 psia) there is a very small Mach Disc and Photo No. 30 (P_n = 88.6 psia) has a distinct Mach Disc. Additional Schlieren photographs in this pressure range, with use of a higher quality light source, should further substantiate this prediction. The close agreement between Addy Ref(12), Schlieren photos 28 through 30 and predictions from the Jet Boundary and Jet Structure Fortran programs further validate the procedure for shock structure prediction presented in this report.

Jet Structure Calculation (Mach Disc Present)

A sample calculation of the Mach Disc structure was provided in Appendix C. This procedure was also programmed into the Jet Structure program. The value of r_d represented the non-dimensional radius of the Mach Disc. From Schlieren Photograph No. 30 this value was (0.45). The Mach Disc radius was plotted as a function of nozzle static pressure ratio in Ref(13). The value is 0.42 for p_j/p_o = 3.2 (P_n = 89.0 psia). The value of L_d from the sample calculation in Appendix C was 3.007. This value was also measured from Schlieren Photo No. 30 and was 3.0. This also agrees with the NASA data in Ref(13).

Values for Mach Disc distance (L_d) and radius (r_d) plotted as functions of nozzle static pressure ratio in Ref(13) were provided in Appendix H. Data from these graphs were curve-fit, resulting in the following equations.

Non-dimensional distance to Mach Disc (L_d):

$$L_d = 0.055 + 1.396\,(p_j/p_o) - 0.198\,(p_j/p_o)^2 + 0.013\,(p_j/p_o)^3 \qquad \text{Eqn(6)}$$

Non-dimensional Mach Disc radius (r_d):

$$r_d = -0.948 + 0.673\,(p_j/p_o) - 0.086\,(p_j/p_o)^2 + 0.0043(p_j/p_o)^3 \qquad \text{Eqn(7)}$$

Curve fitting enables this empirical data to be programmed into the Jet Structure program. The following Table compares L_d and r_d data as calculated by the Jet Structure program, Equation 6 and Equation 7, and measurement from Schlieren photographs.

Table 4
Values of (L_d) and (r_d) as a Function of Pressure Ratio

Photo No.	P_n	p_j/p_o	L_d(prog)	L_d(Eqn 6)	%Dev	L_d(photo)	r_d(prog)	r_d(Eqn 7)	% Dev
----	72.5	2.61	2.81	2.58	8.2	----	----	----	----
29	75.7	2.72	2.85	2.65	6.9	2.8	----	----	----
----	80.0	2.87	2.90	2.75	5.4	----	0.394	0.378	4.1
----	85.0	3.05	2.96	2.85	5.0	----	0.403	0.428	5.8
30	89.0	3.20	3.01	2.93	2.7	2.95	0.402	0.466	13.5
31	95.0	3.41	3.08	3.04	1.3	3.0	0.403	0.514	21.8
----	100.0	3.59	3.14	3.13	0.4	----	0.416	0.555	25.0
----	110.0	3.95	3.28	3.29	0.5	----	0.451	0.593	22.1
----	115.0	4.11	3.35	3.37	0.6	----	0.513	0.663	23.7
----	120.0	4.29	3.43	3.45	0.6	----	0.531	0.695	23.5

From Table 4, the values of Mach Disc distance (L_d) from NASA predictions, Schlieren photographs and the Jet Structure program, agree closely over a wide range of pressure ratios. Values of Mach Disc radius (r_d), however, deviate as much as 25% from NASA experimental data.

Conservation of Mass Across the Mach Disc Structure

The flow properties across the oblique/normal shock wave structure in Regions 4, 5, and 9 were calculated using the Jet Structure program. The dimensions of the Mach Disc structure were calculated in the sample calculation in Appendix C for P_n = 89.0 psia. Recall the Mach Disc structure.

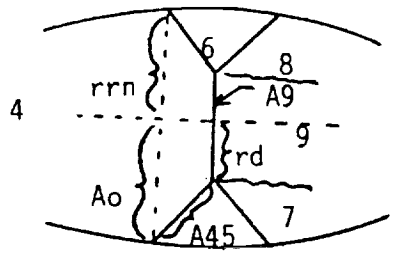

Figure 4a. Mach Disc Structure

Where: A_{45} = surface area of the oblique shock wave
A_0 = vertical component of A_{45}
A_9 = surface area of the normal shock wave

The conservation of mass across an oblique shock wave is expressed as follows Ref(2).

$$\rho_4 V_{n4} = \rho_5 V_{n5} \qquad \text{Eqn(8)}$$

V_n = velocity normal to the oblique shock wave

Normal velocity is related to free stream velocity as follows.

$$V_{n4} = V_4 \sin(\varepsilon_{45})$$

Where (ε_{45}) is the oblique shock wave angle. Expressing V_n in terms of Mach number.

$$V_{n4} = M_4 a_4 \sin(\varepsilon_{45}) = M_4 (\gamma R t_4)^{1/2} \sin(\varepsilon_{45})$$

The normal velocity on the other side of the shock wave (V_{n5}) is related to the free stream velocity in Region 5 as follows.

$$V_{n5} = M_5 a_5 \sin(\varepsilon_{45} - \delta_{45}) = M_5 (\gamma R t_5)^{1/2} \sin(\varepsilon_{45} - \delta_{45})$$

Equation 8 can be rewritten as follows.

$$\rho_4 M_4 (\gamma R t_4)^{1/2} \sin(\varepsilon_{45}) = \rho_5 M_5 (\gamma R t_5)^{1/2} \sin(\varepsilon_{45} - \delta_{45})$$

Writing the continuity equation across the Mach Disc.

$$m_4 = m_5 + m_9$$

Making substitutions.

$$\rho_4 M_4 (\gamma R t_4)^{1/2} A_4 = \rho_5 M_5 (\gamma R t_5)^{1/2} \sin(\varepsilon_{45} - \delta_{45}) + \rho_9 M_9 (\gamma R t_9)^{1/2} A_9 \qquad \text{Eqn(9)}$$

From Figure 6a, A_{45} is realted to A_o as follows.

$$A_{45} = A_o / \sin(\varepsilon_{45})$$

Also from Figure 6a, A_o can be calcualted from the known non-dimensional values r_m and r_d.

$$A_o = \pi (r_m (0.2275))^2 = \pi (r_d (0.2275))^2$$

In the above expression r_m and r_d are made dimensional by multiplying by the nozzle radius (r_n). For the case of P_n = 89.0 psia.

$$r_m = 1.355$$
$$r_d = 0.402$$

Substituting values and solving for A_o, A_{45} and A_9 ($\varepsilon_{45} = 43.2°$).

$$A_o = 0.2725 \text{ in}^2$$
$$A_{45} = 0.3981 \text{ in}^2$$
$$A_9 = 0.026 \text{ in}^2$$

The values of static density, temperature, pressure and Mach number for Regions 4, 5, and 9 were calculated using the Jet Structure program and are as follows.

$\rho_4 = 0.0488$ lbm/ft^3	$\rho_9 = 0.173$
$M_4 = 2.69$	$M_9 = 0.496$
$t_4 = 214.5°R$	$t_9 = 500.3$
$\rho_5 = 0.1184$	
$M_5 = 1.682$	
$t_5 = 335.5$	

After substituting values into Equation 9 the left and right hand sides of the equation balance.

$$0.1956 = 0.1956$$

And mass is conserved across the Mach Disc.

Discussion

Schlieren photograph measurements of Prandtl primary wavelength (w/r_n), Mach Disc radius (r_d) and Mach Disc distance (L_d) consistently agreed with measurements conducted by NASA and presented in Refs(3) and (13). This can be observed by examination of Tables (1) and (4). In addition, little deviation was observed between measurements of Prandtl primary wavelength from photographs of the straight and 15° nozzles at similar pressure ratios.

The oblique shock/expansion wave structure within the jet was calculated by combining the calculated jet boundary contour in the form of a 3rd order polynomial with principles and governing equations of oblique shock/expansion wave interaction and the basic geometry of the jet as illustrated in Figure 2. Sample calculations were provided in Appendix B and C and the Jet Boundary and Jet Structure Fortran programs were written to calculate the jet structures with and without Mach Discs. Results of calculations are presented in Tables 3 and 4.

Figure 3 indicated that the use of the Adamson-Nicholls integral method for calculation of the jet boundary contour resulted in contours close to those determined by the use of the Method of Characteristics. The deviation between the two methods at a pressure ratio of $p_j/p_o = 2.0$ was approximately 4%. Since the pressure ratios encountered in this project were in the range of 1.1 to 3.2, the Adamson-Nicholls method was a sufficient model for jet boundary contours.

The Jet Boundary and Jet Structure programs were combined in order to predict the pressure ratio at which the Mach Disc would first appear in the flow and was calculated as

72.5 psia. This prediction is substantiated by Addy Ref(12), NASA Ref(13) and by the examination of Schlieren photographs taken in this project.

Table 3 summarized the Jet Structure program results for predicted Prandtl primary wavelength (w/r_n) for the case of no Mach Disc present in the jet. The Table also compared these values with those predicted by NASA in Ref(3). The results agree quite closely. Table 4 compared predicted values of Mach Disc distance (L_d) and Mach Disc radius (r_d) using the Jet Structure Program and those determined experimentally by NASA Ref(13). Calculated values of Mach Disc distance (L_d) are consistently in close agreement with NASA empirical data. Analytical prediction of Mach Disc radius, however, deviated as much as 25% from empirical data. Conservation of Mass across the Mach Disc structure was investigated in order to validate flow properties calculated by the Jet Structure program.

Conclusions

Schlieren photography provided an indispensable source of information for comparison with analytical models presented in this report for the prediction of the axisymmetric jet expansion/oblique shock wave structure. However, Schlieren photographs were unable to visualize certain aspects of the flow structure including slip-lines associated with the Mach Disc structure. In addition, there was poor definition of small Mach Discs, particularly in the nozzle total pressure range of 75 psia to 80 psia. These deficiencies can be avoided in future Schlieren photography conducted on the thrust stand with use of a higher quality Schlieren system light source.

The Adamson-Nicholls integral method of computing the contour of the constant pressure jet boundary agreed closely with the Method of Characteristic solution at low pressure ratios. If larger pressure ratios are encountered in subsequent work with the thrust stand, then the accuracy of the calculated jet boundary contour could degrade, resulting in a less precise jet structure approximation. A possible remedy for this problem would be to incorporate a Method of Characteristics solution into the Jet Boundary program. This would allow the two methods to be compared at any supply pressure.

The jet structure calculation method discussed and illustrated by example in Appendix B produced excellent results at pressure ratios at which no Mach Disc formed in the flow. Although the expansion from the nozzle exit was modeled as Prandtl-Meyer expansion (isentropic flow/perfect gas) and the resulting expansion fans were approximated as discrete expansion waves, excellent results were obtained for the Prandtl primary wavelength (w/r_n) estimates.

Calculation of the jet structure with a Mach Disc present required several simplifying assumptions. Recall that in the sample calculation in Appendix C, Equations 30 through 34 provided 5 equations with 7 unknowns. The simplifying assumptions made were that the oblique shock wave angles ε_{45} and ε_{57} were equal and that the Prandtl primary wavelength (w/r_n) was known. Resulting estimates of Mach Disc distance (L_d) were accurate, however, calculated values of Mach Disc radius were not as accurate. The method overall functions well as a means of approximating the Mach Disc structure. No previous analytical work of this kind was found in the review of literature.

List of References

1. Saad, M.A., Compressible Fluid Flow, Prentice Hall, Inc., N.J., 1985.

2. Zucrow, M.J., Hoffman, J.D., Gas Dynamics (Vol. 1), Wiley and Sons, Inc., N.Y., 1976.

3. Love, E.S., Grisby, C.E., Lee, L.P., Woodling, M.J., "Experimental and Theoretical Studies of Axisymmetric Free Jets", NASA TR R-6, 1959.

4. Adamson, T.C., Nicholls, J.A., "On the Structure of Free Jets from Highly Underexpanded Nozzles Into Still Air", *Journal of the Aerospace Sciences,* January 1959.

5. Prandtl, L., Essentials of Fluid Dynamics, Haffner Publ., N.Y., 1952.

6. Pack, D.C., "On the Formation of Shock Waves in Supersonic Gas Jets", *Quarterly Journal of Mechanics and Applied Mathematics,* 1947.

7. Bleakney, W., Taub, A.H., "Interaction of Shock Waves", *Reviews of Modern Physics,* October 1949.

8. Wilcox, D.E., Weir, A., Nicholls, J.A., "Location of Mach Discs and Diamonds in Supersonic Jets", *Journal of Aeronautical Sciences,* February 1957.

9. Thompson, P.A., Compressible Fluid Dynamics, McGraw-Hill Co., N.Y., 1972.

10. Merzkirch, W., Flow Visualization (2nd Edition), Academic Press, Inc., N.Y., 1987.

11. Gerald, C.F., Wheatley, P.O., Applied Numerical Analysis (4th Edition), Addison-Wesley Publishing Company, N.Y., 1989.

12. Addy, A.L., "Effects of Axisymmetric Nozzle Geometry on Mach Disk Characteristics, *AIAA Journal,* Vol. 19, No. 1, January 1981.

13. Vick, A.R., Andrews, E.H., "Comparison of Experimental Free Jet Boundaries with Theoretical Results Obtained with the Method of Characteristics", NASA TN D-2327, June 1964.

14. Ladenburg, R.N., Physical Measurements in Gas Dynamics and Combustion, High Speed Aerodynamics and Jet Propulsion (Vol. IX), Princeton University Press, N.J., 1954.

15. Dean, R.J., Aerodynamic Measurements, Gas Turbine Laboratory, Massachusetts Institute of Technology, Eagle Enterprises, N.Y., 1957.

16. Andersen, J.D., Modern Compressible Flow with Historical Prospective, McGraw Hill Book Company, N.Y., 1982.

17. Cheer, F., Elements of Compressible Flow, John Wiley and Sons, Ltd., N.Y., 1963.

18. White, F.M., Fluid Mechanics, McGraw Hill Book Company, N.Y., 1979.

19. Pai, S., Fluid Mechanics of Jets, D. Van Nostrand Company, Inc., N.Y., 1954.

20. Mark, H., "The Interaction of a Reflected Shock Wave with the Boundary Layer in a Shock Tube", NACA TM 1418, March 1958.

21. Bazhenova, T.V., Gvozdeva, L.G., "Shock Waves in Real Gases", NASA TT F-585, October 1969.

22. Oswatitsch, K., Gas Dynamics, Academic Press, Inc., N.Y., 1956.

23. Benedict, R.P., Fundamentals of Gas Dynamics, John Wiley and Sons, Inc., N.Y., 1983.

24. Addy, A.L., "Effects of Axisymmetric Sonic Nozzle Geometry on Mach Disk Characteristic", *AIAA Journal,* Vol. 19, No., 1, January 1981.

25. Fox, J.H., "On the Structure of Jet Plumes", *AIAA Journal,* Vol. 12, No. 1, January 1974.

26. Crist, S. Sherman, P.M., Glass, D.R., "Study of Highly Underexpanded Free Jets", *AIAA Journal,* Vol. 4, No. 1, January 1966.

27. Abett, M., "Mach Disks in Underexpanded Exhaust Plumes", *AIAA Journal,* Vol. 9, No. 3, March 1971.

28. Eastman, D.W., "Location of the Normal Shock Wave in the Exhaust Plume of a Jet", *AIAA Journal,* Vol. 1, No. 4, April 1963.

29. Chuech, S.G., Lau, M.C., Faeth, G.M., "Structure of Turbulent Sonic Underexpanded Free Jets", *AIAA Journal,* Vol. 27, No. 4, April 1963.

30. Thornock, R.L., Brown, E.F., "An Experimental Study of Compressible Flow Through Convergent-Conical Nozzles, Including a Comparison with Theoretical Results", Transactions of the ASME, *Journal of Basic Engineering,* December 1972.

31. Shapiro, A.H., The Dynamics and Thermodynamics of Compressible Fluid Flow, John Wiley and Sons, N.Y., 1953.

32. Courant, R., Fredrichs, K.D., Supersonic Flow and Shock Waves, Interscience Publishing, Inc., N.Y., 1948.

33. Liepmann, H.W., Puckett, A.E., Introduction of Aerodynamics of a Compressible Fluid, John Wiley and Sons, N.Y., 1947.

34. Walz, A., Boundary Layers of Flow and Temperature, M.I.T. Press, Cambridge, Mass., 1969.

35. Schlichting, H., Boundary Layer Theory (7th Edition), McGraw-Hill Book Company, N.Y., 1979.

36. Schetz, J.A., Foundations of Boundary Layer Theory of Momentum, Heat and Mass Transfer, Prentice Hall, Inc., N.J., 1984.

37. Wesoky, H.L., "Boundary Layer Measurements in Accelerated Flows Near Mach 1", NASA TN D-3882, 1967.

38. Wesoky, H.L., May, C., "Boundary Layer Measurements in an Accelerated Flow With and Without Heat Transfer", NASA TN D-7030, 1971.

39. Pai, S., Viscous Flow Theory, D. Van Norstrand Co., Inc., Princeton, N.J., 1956.

40. Hoffman, J.D., "Approximate Analysis of Non-isentropic Flow in Conical Nozzles", *Journal of Spacecraft and Rockets*, Vol. 6, No. 11, December 1969.

41. Scofield, M.P., Hoffman, J.D., "Optimization of Conical Thrust Nozzles", *Journal of Spacecraft and Rockets*, Vol. 4, No. 11, 1967.

42. Durham, F.P., "Thrust Characteristics of Underexpanded Nozzles", *Jet Propulsion*, December 1955.

43. Cambel, A., Jennings, B., Gas Dynamics, McGraw Hill Book Company, Inc., N.Y., 1958.

44. Sheeran, W.J., Dusanjh, D., "Observations on Jet Flows from a Two-Dimensional Underexpanded Jet", *AIAA Journal*, Vol. 6, No. 3, March 1968.

Appendix A

Review of Gas Dynamics

Prandtl-Meyer Expansion/Initial Jet Boundary Angle (α)

When the air initially expands to atmospheric pressure at the nozzle exit in the underexpanded converging nozzle, it is assumed to encounter a Prandtl-Meyer expansion. In Prandtl-Meyer expansion air behaves as a perfect gas expanding isentropically from an original Mach number of 1.0 or greater to a region of lower static pressure and consequently higher Mach number. This is illustrated in Figure 8.

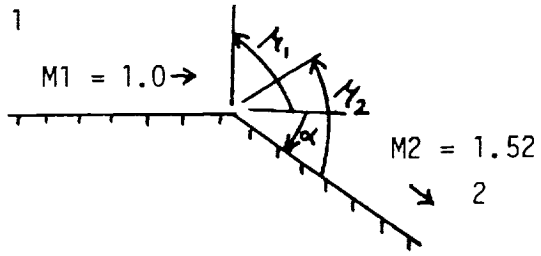

Figure 8. Expansion of a Sonic Flow

In Figure 8, (μ_1) is the Mach line angle associated with Region 1 (90° for M = 1.0), (μ_2) is the Mach line angle in Region 2 and (δ) is the flow turning angle. The governing equation for Prandtl-Meyer expansion is as follows, Ref(4).

$$\delta = \nu_2 - \nu_1 = -(b)^{1/2} \{ \tan^{-1} [(M_2^2 - 1.0)/b]^{1/2} - \tan^{-1} [(M_1^2 - 1.0)/b]^{1/2} \} + [\tan^{-1} (M_2^2 - 1.0)^{1/2} - \tan^{-1} (M_1^2 - 1.0)^{1/2}]$$

In this equation (ν_1) is the Prandtl-Meyer angle in Region 1 (0° for M = 1.0), (ν_2) is the Prandtl-Meyer angle in Region 2. In the case of $M_1 = 1.0$, the equation simplifies as follows.

$$\alpha = \nu_2 = -(b)^{1/2} \tan^{-1} [(M_2^2 - 1.0)/b]^{1/2} + \tan^{-1}(M_2^2 - 1.0)^{1/2} \qquad \text{Eqn(1)}$$

Where:

$$b = \frac{\gamma + 1}{\gamma - 1}$$

In Equation 1, ν_2 is replaced by α to avoid confusion in subsequent calculations. This equation gives the initial turning angle of the flow at the nozzle exit. As discussed earlier, this is the maximum slope of the constant pressure jet boundary. There are two unknowns in Equation 1, M_2 and α.

The Mach number in Region 2 can be solved for readily since the flow is assumed to be isentropic during expansion. Total (stagnation) pressure in the nozzle is measured with a Pitot tube on the thrust stand located at the entrance to the nozzle. In the isentropic expansion of an ideal gas, Mach number and total to static pressure ratio are related as follows.

$$P/p = (1.0 + \frac{\gamma - 1}{2} M^2)^{(\gamma-1)/\gamma} \qquad \text{Eqn(10)}$$

In Equation 10, (P) is the total pressure, (p) is the static pressure, (M) is the Mach number. Solving for the Mach number.

$$M = (\frac{2}{\gamma - 1} [(P/p)^{(\gamma-1)/\gamma} - 1.0])^{1/2} \qquad \text{Eqn(10a)}$$

Since the final Mach number is known, Equation 1 can be solved for the initial flow direction of the jet boundary. Initial boundary flow angle increases as inlet pressure increases.

Principles of Expansion Wave/Oblique Shock Wave Interaction

The most important concepts associated with expansion wave and oblique shock wave reflection and interaction are as follows Ref(4).

Expansion Waves:

1. An expansion wave turns the flow away from itself.
2. Expansion waves reflect from solid surfaces as expansion waves.
3. Expansion waves reflect from a free pressure boundary as oblique shocks.

Oblique Shock Waves:

1. An oblique shock wave turns the flow toward itself.
2. Oblique shock waves reflect from a solid surface as oblique shocks.
3. Oblique shocks reflect from a free pressure boundary as expansion waves.

Derivation of the Maximum Flow Deflection Angle (δ_{max})

The Mach Disc forms when an oblique shock wave with a large deflection angle (δ) generates a reflected shock with a corresponding deflection angle greater than $(\delta)_{max}$. When the deflection angle corresponding to the Mach number in Region 5 (behind the incident oblique shock) exceeds $(\delta)_{max}$, the Mach Disc will form. The maximum deflection angle associated with an oblique shock is obtained in the following manner. The geometry of flow through an oblique shock wave is illustrated in Figure 9.

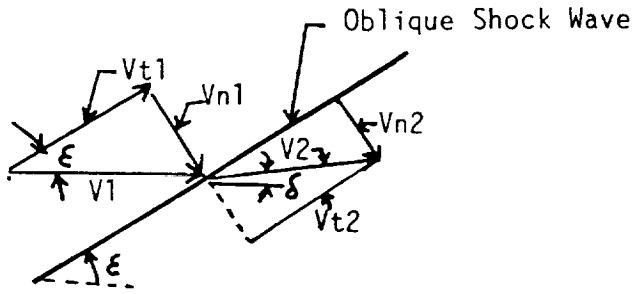

Figure 9. Flow Geometry Across an Oblique Shock Wave

Upon inspection of Figure 9, the flow deflection angle (δ) can be defined in terms of velocities as follows.

$$\delta = \tan^{-1} (V_t/V_{n2}) - \tan^{-1} (V_t/V_{n1})$$

Where V_t and V_n are tangent and normal velocity components, respectively. Recall for an oblique shock wave that the tangential velocity remains constant across the shock. (δ_{max}) can be calculated by differentiating (δ) with respect to V_t in the above expression and setting it equal to zero. After differentiating, δ_{max} occurs when:

$$V_t/V_{n1} = (V_{n2}/V_{n1})^{1/2}$$

Substituting into the equation for δ.

$$\delta_{max} = \tan^{-1} (V_{n1}/V_{n2})^{1/2} - \tan^{-1} (V_{n1}/V_{n2})$$

From the governing equations of oblique shock waves.

$$V_{n1}/V_{n2} = \rho_2/\rho_1 = r$$

Substituting

$$\delta_{max} = \tan^{-1} (r)^{1/2} - \tan^{-1} (r)^{-1/2}$$

Employing a trig identity and rearranging.

$$\delta_{max} = \tan^{-1} \frac{r - 1}{2(r)^2} \qquad \text{Eqn(5)}$$

If the flow turning angle associated with a given Mach number is greater than δ_{max}, then a regular Mach reflection is not possible and a Mach Disc consequently forms. Ref(7) presents an excellent development of Mach Disc or Mach reflection.

Appendix B

Sample Calculation (No Mach Disc)

Sample Calculation of Jet Structure (No Mach Disc)

In reference to Figure 2, the shock structure within the constant pressure boundary of an underexpanded jet can now be calculated. In this sample calculation the ratio of nozzle exit static pressure to ambient pressure is 2.0. For a constant specific heat ratio of $\gamma = 1.4$, Equation 3a can be written as follows:

$$M_2 = [\ (5.0((P/p)^{0.2857} - 1.0)\ ]^{1/2}$$

For $p_j/p_o = 2.0$, p_j is then 29.4 psia. In order for the flow to choke, the pressure must exceed the critical pressure ratio of $P/p = 0.52828$. The flow will therefore be choked for any nozzle total pressure greater than 27.8 psia which is the case in this example. For $p_j/p_o = 2.0$, $P/p = 3.8$. Solving Equation 10a for M_2.

$$M_2 = 1.52$$

Substituting this value of Mach number into Equation 2, the initial turning angle of the flow is 12.5°. The next step is to determine the angle of the initial Mach wave.

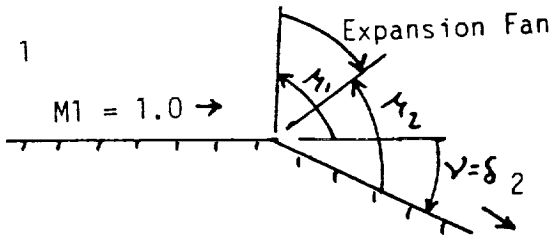

Figure 10. Prandtl-Meyer Expansion

Recall from Prandtl-Meyer expansion Ref(2).

$$\tan(\mu) = 1.0/(M^2 - 1.0)^{1/2}$$

or

$$\mu = \tan^{-1} [\ 1.0/(M^2 - 1.0)^{1/2}\ ] \qquad \text{Eqn(11)}$$

In Equation 11, (μ) is the Mach angle. For $M_1 = 1.0$ using Equation 11, (μ_1) = 90° and $M_2 = 1.52$, (μ_2) = 41.1°. From Figure 10, the average of (μ_1) and (μ_2) measured from the horizontal axis is:

$$\mu_{ave} = \frac{\mu_1 + (\mu_2 - \alpha)}{2} \qquad \text{Eqn(12)}$$

Substituting values (μ_{ave}) = 59.3°. This is the angle the first expansion wave makes with respect to the horizontal axis. Referring once again to Figure 2 as the flow travels from Region 3 to 4 it passes through a reflected expansion wave. From Prandtl-Meyer expansion theory the flow deflection angle (α) is related to the initial and final Prandtl-Meyer angles as follows.

$$\alpha = \nu_2 - \nu_1$$

or this case:

$$\alpha_{24} = \nu_4 - \nu_2$$

(ν_2) was calculated before from Equation 1 as 12.5°. The initial flow turning angle was 12.5° so (ν_4) was calculated as:

$$\nu_4 = 12.5 + 12.5 = 25°.$$

with (ν_4), (ν_2), and (M_2) known, Equation 1 can be solved implicitly for M_4.

$$M_4 = 1.95.$$

The average Mach angle or discrete Mach wave for Region 2 to 4 was solved in a similar as that from 1 to 2. However, it is important to keep track of the relationship between these angles and the flow axis.

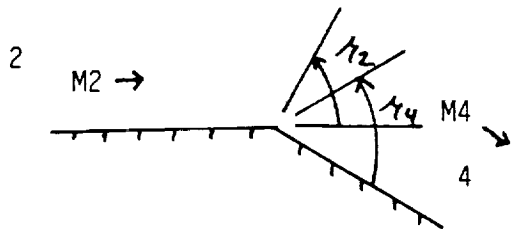

Figure 11. Expansion From Flow Region 2 to 4

Substituting values for M_2 an M_6 into Equation 11, (μ_2) = 41.1 + 12.5 = 53.6°, (μ_4) = 43.2°. The average Mach wave from Region 2 to 4 is 48.6° with respect to the horizontal axis. Recalling the shock structure from Region 2 to 4.

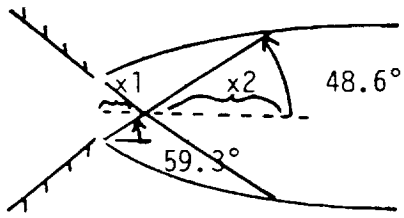

Figure 12. Jet Structure From Flow Region 2 to 4

In Figure 12, the non-dimensional distance x_1/r_n is easily solved for as $x_1 = r_n/\tan(59.3)$ or $x_1/r_n = 0.593$. The distance x_2/r_n can be solved for, knowing the equation for the curved boundary. The jet boundary solution for $p_j/p_o = 2.0$ from the Jet Boundary Fortran program was put into a curve fitting program and the following 3rd order polynomial was generated.

$$r/r_n = 1.0 + 0.225(x/r_n) - 0.137(x/r_n)^2 + 0.033(x/r_n)^3 \qquad \text{Eqn(13)}$$

There are 2 unknowns in Equation 13, r/r_n and x/r_n. Another expression relating x/r_n and r/r_n can be developed upon inspection of Figure 12.

$$x/r_n = x_1/r_n + x_2/r_n = 0.593 + x_2/r_n$$
$$x_2/r_n = (r/r_n)/\tan(48.5)$$

Combining both equations to get one equation in terms of r/r_n and x/r_n:

$$r/r_n = \tan(48.5)(x/r_n - 0.593) \qquad \text{Eqn(14)}$$

Combining Equations 13 and 14 and solving for x/r_n and r/r_n:

$$x/r_n = 1.61; \quad r/r_n = 1.15$$

Up to this point the flow is assumed to be isentropic since it has only encountered expansion waves. The static pressure at location 4 can then be calculated using isentropic and expansion process.

$$p_4/P_4 = (1.0 + ((\gamma - 1)/2)\, M_4)^{(\gamma-1)/(\gamma)} \qquad \text{Eqn(15)}$$

Where (γ) = 1.4, M_4 = 1.95, $P_4 = P_n$ = 55.65 psia. Substituting values (p_4 = 7.69 psia). Recall from the general principles of expansion waves that an expansion wave reflects from a free pressure boundary as an oblique shock wave. The static pressure in Region 4 is less than atmospheric. The flow must therefore encounter an oblique shock wave in order to raise its pressure to atmospheric pressure in Region 6 and maintain the constant pressure boundary.

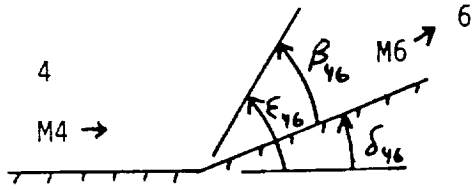

Figure 13. Oblique Shock Wave Structure

In Figure 13, (δ) is the flow turning angle, (ϵ) is the oblique shock wave angle with respect to the original flow axis, and (β) is the angle of the oblique shock wave with respect to the flow direction on the other side of the shock wave. From Ref(2), the governing equations for property change across oblique shocks are as follows.

$$p_6/p_4 = \frac{2\gamma}{\gamma + 1} M_4^2 \sin^2(\epsilon_{46}) - \frac{\gamma - 1}{\gamma + 1} \qquad \text{Eqn(16)}$$

Static density ratio:

$$\rho_6/\rho_4 = \frac{(\gamma + 1) M_4^2 \sin^2(\epsilon_{46})}{2 + (\gamma - 1) M_4^2 \sin^2(\epsilon_{46})} \qquad \text{Eqn(17)}$$

Relationship between flow turning angle (δ) and oblique shock angle (ε):

$$1/\tan(\delta) = \left[\frac{(\gamma + 1)}{2} \quad \frac{M_4^2}{M_4^2 \sin^2(\varepsilon_{46}) - 1} - 1 \right] \tan(\varepsilon_{46}) \qquad \text{Eqn(18)}$$

Mach number on the other side of an oblique shock:

$$\frac{\tan(\varepsilon_{46})}{\tan(\beta_{46})} = \left(\frac{2}{\gamma + 1} \right) \left(\frac{1}{M_6^2 \sin^2(\beta_{46})} + \frac{\gamma - 1}{2} \right) \qquad \text{Eqn(19)}$$

In the above equation, the unknowns are (ε_{46}), (ρ_6), (δ_{46}), (M_6) and (β_{46}). In most problems involving oblique shock waves there is something known on the other side of the shock. It is usually the flow turning angle (δ). In this case the static pressure in Region 6 is known and is atmospheric. The procedure for solving for the unknowns from the above equations is as follows.

1. Solve Equation 16 for the oblique shock wave angle (ε_{46}).

2. Solve Equation 18 implicitly for the flow turning angle (δ_{46}). Solve for (β_{46}). (β_{46}) = (ε_{46}) - (δ_{46}).

3. Solve Equation 19 implicitly for M_6.

For (γ = 1.4) Equation 16 can be rewritten as follows.

$$p_6/p_4 = 1.1666\, M_4^2 \sin^2(\varepsilon_{46}) - 0.1666$$

Where p_6 = 14.7 psia, p_4 = 7.69 psia and M_4 = 1.95. Solving for (ε_{46}), (ε_{46}) = 43.2°

Solving Equation 18 for (δ_{46}) and using ($\gamma = 1.4$).

$$\delta_{46} = \tan^{-1} \left[\left(\frac{1.2\, M_4^2}{M_4^2 \sin^2(\varepsilon_{46}) - 1} - 1 \right) \tan(\varepsilon_{46}) \right]^{-1}$$

$$(\delta_{46}) = 12.42^\circ;\ (\beta_{46}) = (\varepsilon_{46}) - (\delta_{46}) = 30.8^\circ$$

Solving Equation 19 for M_6.

$$M_6 = \left[\left(\frac{\tan(\varepsilon_{46})}{0.833 \sin^2(\beta_{46})} - 0.2 \right) \sin^2(\beta_{46}) \right] = 1.50$$

In this region of the jet, two oblique shock waves of equal strength intersect at the centerline of the flow stream. When oblique shocks of equal strength intersect, the problem is treated in the same manner as a normal reflection from a solid surface Ref(1). The flow deflection angle (δ_{67}) cannot exceed the maximum flow deflection angle $(\delta)_{max}$. Recall from the discussion of Mach Disc formation and Equation 5 that $(\delta)_{max}$ is defined as follows.

$$\delta_{max} = \tan^{-1} \frac{r - 1}{2(r)^2} \qquad r = \rho_7/\rho_6$$

and (ρ_7/ρ_6) from Equation 17 is

$$r_{67} = \rho_7/\rho_6 = \frac{(\gamma + 1) M_6^2 \sin^2(\varepsilon_{67})}{2 + (\gamma - 1) M_6^2 \sin^2(\varepsilon_{67})}$$

In this equation there are two unknowns (ε_{67}) and (r_{67}). (ε_{67}) corresponds to the maximum oblique shock wave angle $(\varepsilon)_{max}$ and is found by differentiating Equation 18, setting it equal zero and solving for $(\varepsilon)_{max}$.

$$\sin^2(\varepsilon_{max}) = \frac{1}{\gamma M_6^2}\left\{\frac{((\gamma+1)M_6^2-1)}{4} + \left[(\gamma+1)\left(1+\frac{(\gamma-1)M_6^2}{2}+\frac{\gamma+1}{16}M_6^4\right)\right]^{1/2}\right\}$$

Eqn(20)

Substituting for M_6 $(\varepsilon)_{max} = 66.5°$. Solving Equation 12 for r_{67} and solving Equation 5 for $(\delta)_{max}$.

$$r_{67} = 1.617 \qquad (\delta)_{max} = 14.5°$$

The value of $(\delta)_{max}$ is greater then (δ_{67}), 12.5° and consequently there is no formation of a Mach Disc. The reflected shock from Region 6 to 7 is therefore strong enough to straighten the flow parallel to the centerline axis. The only known property in Region 7 is therefore the flow deflection angle. That is $(\delta_{45}) = (\delta_{67}) = 12.42°$. Looking at Equations 16 through 19 and knowing (δ_{67}), Equation 18 can be solved implicitly for (ε_{67}). $(\varepsilon_{67}) = 65.3°$. Substituting into Equation 16 and solving for p_7.

$$p_7 = p_6(1.166\,M_6^2\sin^2(\varepsilon_{67}) - 0.166)$$

$$p_7 = 29.5 \text{ psia}$$

Note that p_7 is higher than atmospheric pressure which is expected since the flow passed through an oblique shock from Region 6 to 7. The final step in this problem is to calculate where the reflected shock wave will intersect the jet boundary. Figure 2 is repeated at this time for clarification.

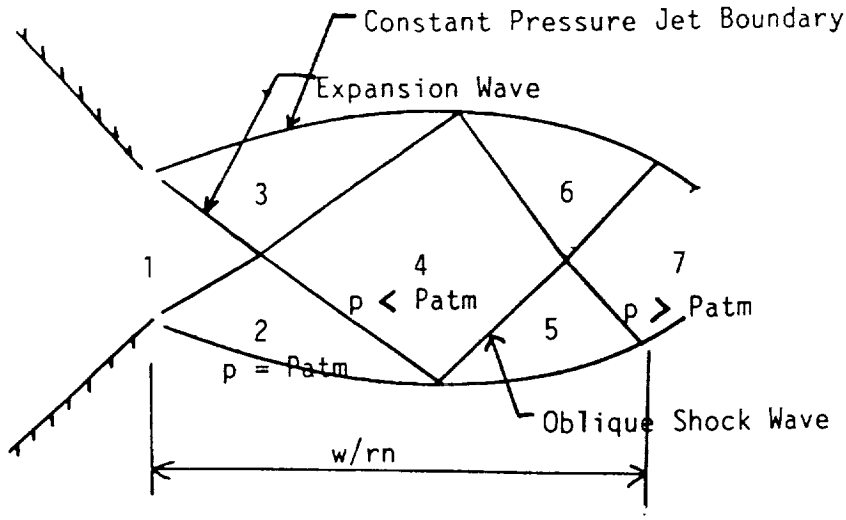

Figure 2. Jet Structure of an Axisymmetric Jet Exhausting Into Still Air

Recall from the previous discussion that the inflection point occurs where the expansion wave reflects from the free pressure boundary. Beyond this point, the curvature of jet boundary is assumed to be the mirror image of the boundary up to the point of inflection. Recall Equation 13.

$$r/r_n = 1.0 + 0.225\,(x/r_n) - 0.137\,(x/r_n)^2 + 0.033\,(x/r_n)^3$$

The non-dimensional distance $(x_1 + x_2)$ was calculated earlier as (1.61). Rewriting Equation 13 so that the boundary beyond the point of inflection is the mirror image of the boundary before the inflection point.

$$r/r_n = 1.0 + 0.225(1.61 - x/r_n) - 0.137(1.61 - x/r_n)^2 + 0.033\,(1.61 - x/r_n)^3 \qquad \text{Eqn(21)}$$

where $x/r_n = x_3 + x_4$

The value of r/r_n is the value at the inflection point and was calculated earlier ($r/r_n = 1.355$).

From Figure 12:

$$x_3 = (r/r_n)/\tan(\varepsilon_{46}) \qquad \text{Eqn(22)}$$

$$x_4 = (r/r_n)/\tan(\beta_{67}) \qquad \text{Eqn(23)}$$

Where $\beta_{67} = \varepsilon_{67} - \delta_{67} = 65.3 - 12.5 = 52.9°$

Substituting x_3 into the x/r_n expression

$$x/r_n = x_3 + x_4 = (r/r_n)/\tan(\varepsilon_{46}) + x_4 \qquad \text{Eqn(24)}$$

The value of r/r_n at location 3 is the value at the point of inflection ($r/r_n = 1.145$). Recall that ($\varepsilon_{46} = 42.3°$)

Solving Equation 22 for x_3

$$x_3 = (1.145)/\tan(43.2) = 1.219$$

Substituting x_3 into Equation 24

$$x/r_n = 1.219 + x_4 \qquad \text{Eqn(25)}$$

Looking at Equations 21, 23 and 25 there are 3 unknowns, x/r_n, x_4 and r/r_n. Solving these equations simultaneously for the unknowns.

$$x_4 = (0.335) \qquad r/r_n = (1.069)$$

$$x/r_n = x_3 + x_4 = 0.335 + 1.219 = 1.554$$

x/r_n (total non-dimensional distance in x direction) $= x_1 + x_3 + x_4$

$$x/r_n \text{ (total)} = w/r_n = 1.61 + 1.554 = 3.16$$

The distance (w/r_n) represents the point at which the reflected oblique shock wave meets the free pressure boundary.

Appendix C

Sample Calculation (Mach Disc Present)

Sample Calculation of Jet Structure (Mach Disc Present)

Amending Figure 4 slightly.

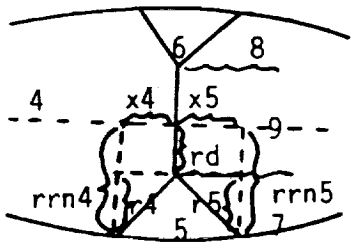

Figure 4. Mach Disc Structure

In Figure 4b, Regions 4, 5, and 6 coincide those in Figure 2. The values of static pressure, temperature and Mach number in Regions 4, 5, and 6 are calculated in the same manner as before. As the flow travels from Region 4 to 9 it passes through a normal shock. The following are the governing equations for property change across a normal shock wave.

Static pressure ratio:

$$\rho_9/\rho_4 = \frac{(2\gamma)\ M_4^2}{\gamma + 1} - \frac{\gamma - 1}{\gamma + 1} \qquad \text{Eqn(26)}$$

Static density ratio:

$$\rho_9/\rho_4 = \frac{(\gamma + 1)\ M_4^2}{2 + (\gamma - 1)M_4^2} \qquad \text{Eqn(27)}$$

Static temperature ratio:

$$t_9/t_4 = \left(\frac{2\gamma\ M_4^2}{\gamma+1} - \frac{\gamma-1}{\gamma+1}\right)\left(\frac{\gamma-1}{\gamma+1} + \frac{2}{(\gamma+1)M_4^2}\right) \qquad \text{Eqn(28)}$$

Mach number on the other side of a Normal Shock:

$$M_9 = \left[\frac{M_4^2 + 2/(\gamma-1)}{(2\gamma/(\gamma-1))M_4^2 - 1}\right]^{1/2} \qquad \text{Eqn(29)}$$

As seen in Figure 4b, the Mach numbers in Regions 7, 8, and 9 are different. The only flow property in common between Regions 7, 8, and 9 is the static pressure. From symmetry the flow properties in Regions 7 and 8 will be the same. The procedure for calculating the flow properties in Regions 7, 8, and 9 is as follows.

1. Solve for flow properties in Regions 4, 5 and 6 as before ($p_5 = p_4 = p_{atm}$).

2. With p_4 and M_4 known, use Equation 26 to solve for p_9.

3. Use Equations 27, 28 and 29 to solve for ρ_9, t_9 and M_9.

4. Since $p_7 = p_9$ use Equation 16 to solve for the oblique shock wave angle (ε_{57}).

5. With M_5 and (ε_{57}) known, use Equation 18 to solve for the flow turning angle (δ_{57}) implicitly. Verify that this angle is less that $(\delta)_{max}$ at that nozzle pressure.

6. Use Equation 19 to solve for M_7 implicitly. Recall that (β_{57}) = (ε_{57}) - (δ_{57}).

Static pressure, temperature, density and Mach number in all regions up to Region 9 are now known. The next step is to determine the size and location of the Mach Disc.

If the Prandtl primary wavelength (w/r_n) is known by actual measurement from a Schlieren photographs or by use of Equation 4, then the structure of the Mach Disc can be determined using the data calculated in the Jet Boundary and Jet Structure Fortran programs. The flow properties in Regions 4, 5, 7 and 9 were calculated using the Jet Structure program. From symmetry, properties in Regions 6 and 8 are equal to those in 5 and 7, respectively. The non-dimensional distance x/r_n is also known for the case of nozzle total pressure of 89.0 psia ($p_j/p_o = 3.2$). The calculated properties are as follows.

$(\varepsilon_{57}) = 42.4°$ $\quad$ $(\varepsilon_{45}) = 43.2°$

$x/r_n = 1.99$

$w/r_n = 4.05$ (Eqn 4)

$w/r_n = 3.95$ (measured from Schlieren Photo No. 30)

If the Prandtl primary wavelength is taken as 4.05 then from Figure 4b.

$$x_4 + x_5 = w/r_n - x/r_n = 4.05 - 1.99 = 2.0 \qquad \text{Eqn(30)}$$

$$x_4 = r_4/\tan(\varepsilon_{45}) \qquad \text{Eqn(31)}$$

$$x_5 = r_5/\tan(\varepsilon_{57}) \qquad \text{Eqn(32)}$$

$$r_{m4} = r_4 + r_d = 1.355 \text{ (from Jet Structure Program)} \qquad \text{Eqn(33)}$$

$$r_{m5} = r_5 + r_d \qquad \text{Eqn(34)}$$

There are 6 unknowns and 5 equations. The unknowns are x_4, x_5, r_4, r_5, r_{m5} and r_d. However, since the angles ε_{45} and ε_{57} are approximately equal the non-dimensional radii r_{m4} and r_{m5} will be approximately equal.

$r_{m4} = r_{m5} = 1.355$

If r_{m5} is known then Equations 30 through 34 reduce to 5 equations and 5 unknowns. The procedure for solving these equations is as follows.

1. Substitute Equation 31 and 32 into 30.

2. Solve Equations 33 and 34 for r_4 and r_5 and substitute into Equation 30.

3. Solve new Equation 30 for r_d.

4. Solve for the remaining unknowns.

The values of the unknowns are as follows.

$x_4 = 1.017$ $\qquad$ $x_5 = 1.047$

$r_4 = 0.955$ $\qquad$ $r_5 = 0.955$

and $\qquad r_d = 0.4$

The value $x_m + x_4$ is the distance from the nozzle to the Mach Disc. In this case:

$$L_d = x_m + x_4 = 1.99 + 1.017 = 3.007$$

This value is also measured from the Schlieren photograph and is 3.0. This also agrees with the NASA data in Ref(13).

Appendix D

Schlieren Photographs

Schlieren Photographs

P_n = Nozzle Total Pressure
p_j = Nozzle Exit Static Pressure
p_o = Atmospheric Pressure (14.7 psia)

Photo No.	P_n (psia)	p_j/p_o
1	32.4	1.164
2	35.4	1.272
3	41.9	1.506
4	51.8	1.862
5	57.8	2.077
6	66.2	2.379
7	67.5	2.426
8	75.2	2.703
9	79.8	2.868
10	88.7	3.188
11	96.1	3.454
12	32.0	1.150
13	35.0	1.258
14	42.1	1.513
15	53.0	1.905
16	58.7	2.109
17	66.3	2.383
18	68.0	2.444
19	76.6	2.753
20	79.8	2.868
21	89.5	3.216
22	31.9	1.146
23	35.6	1.279
24	41.2	1.481
25	52.2	1.876
26	57.8	2.077
27	66.5	2.389
28	68.4	2.458
29	75.6	2.717
30	88.6	3.184
31	97.0	3.486
32	32.1	1.154
33	35.5	1.276
34	41.7	1.499
35	52.0	1.869
36	55.2	1.984

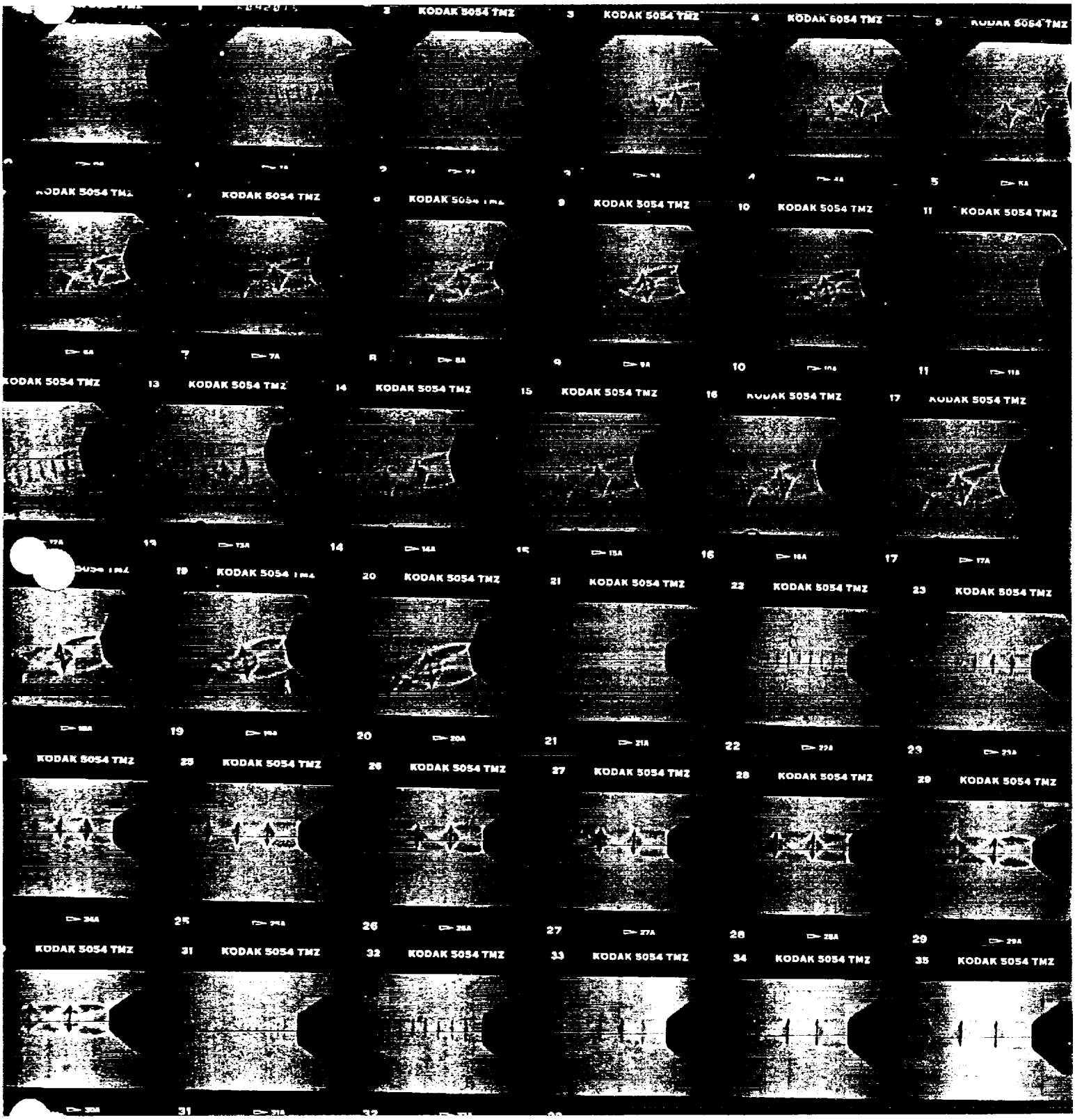
KODAK 5054 TMZ

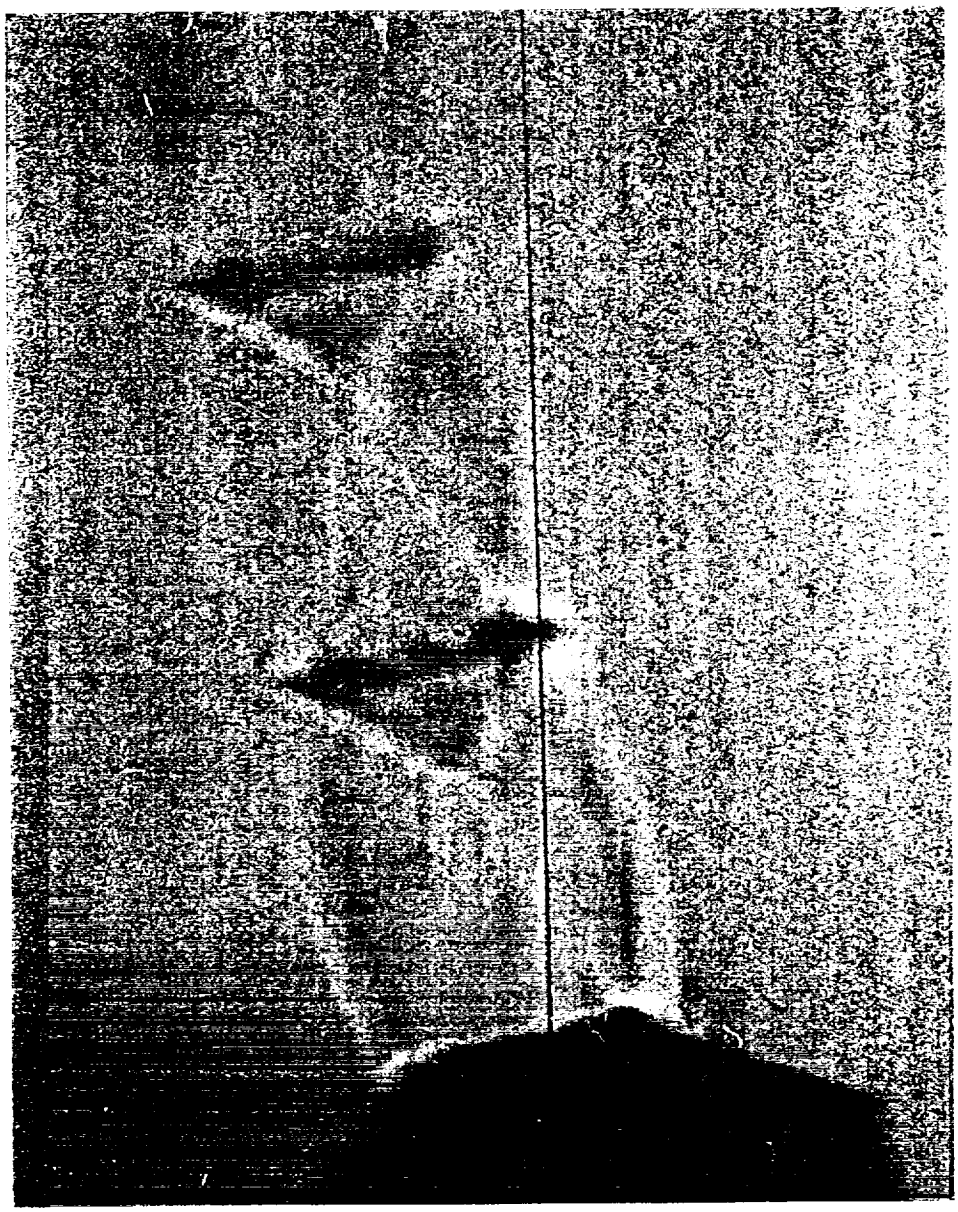

Schlieren Photo No. 18

Pn = 68.0psia

Schlieren Photo No. 19

$P_n = 76.6$ psia

Schlieren Photo No.21

P_n = 89.5 psia

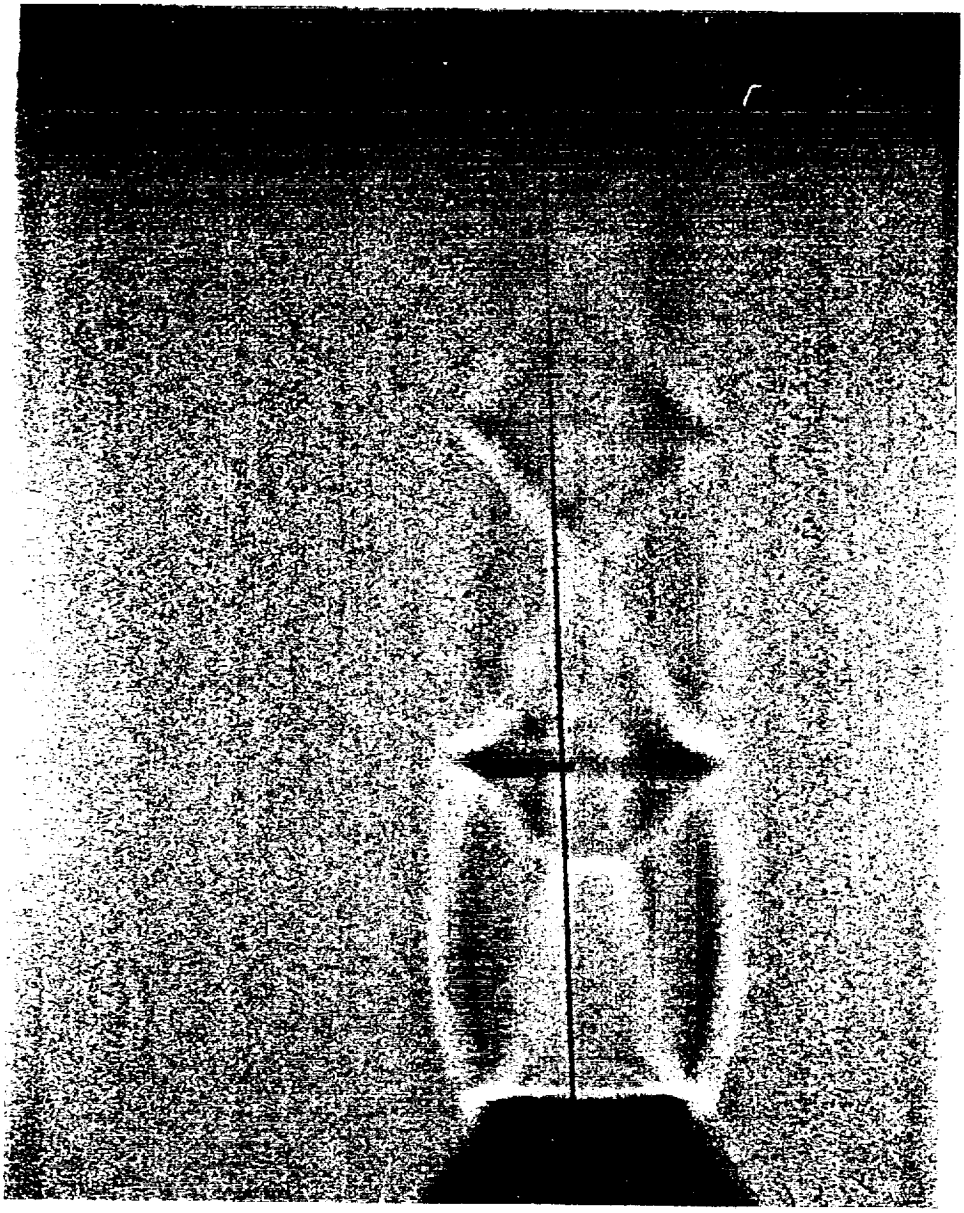

Schlieren Photo No. 31

Pn = 97.0 psia

Appendix E

Calculated Jet Boundary Contours

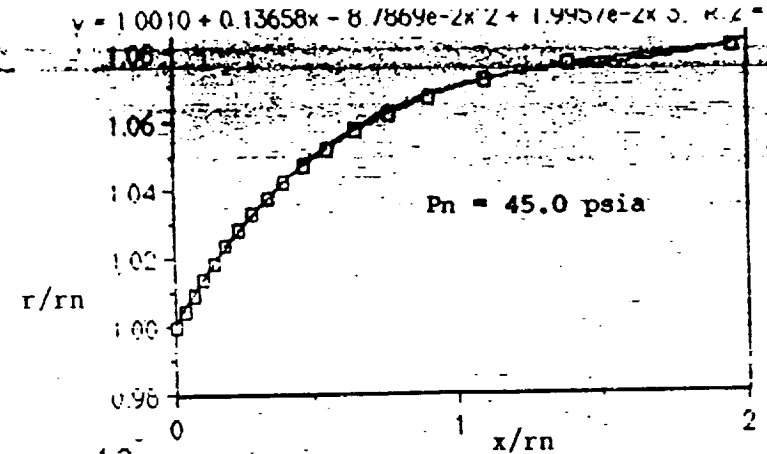
y = 1.0010 + 0.13658x - 8.7869e-2x^2 + 1.9957e-2x^3 R^2 = 0.999
1.08
1.06
1.04
1.02
1.00
0.96
r/rn
Pn = 45.0 psia
0
1
2
x/rn

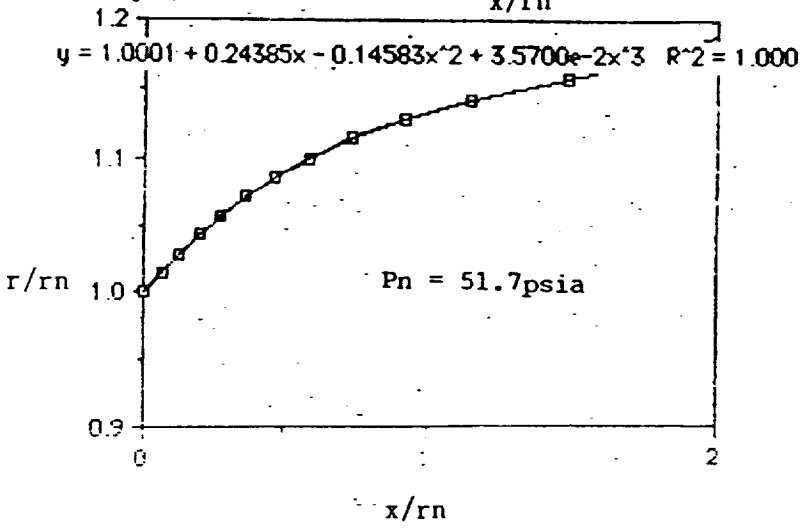
1.2
y = 1.0001 + 0.24385x - 0.14583x^2 + 3.5700e-2x^3 R^2 = 1.000
1.1
1.0
0.9
r/rn
Pn = 51.7psia
0
2
x/rn

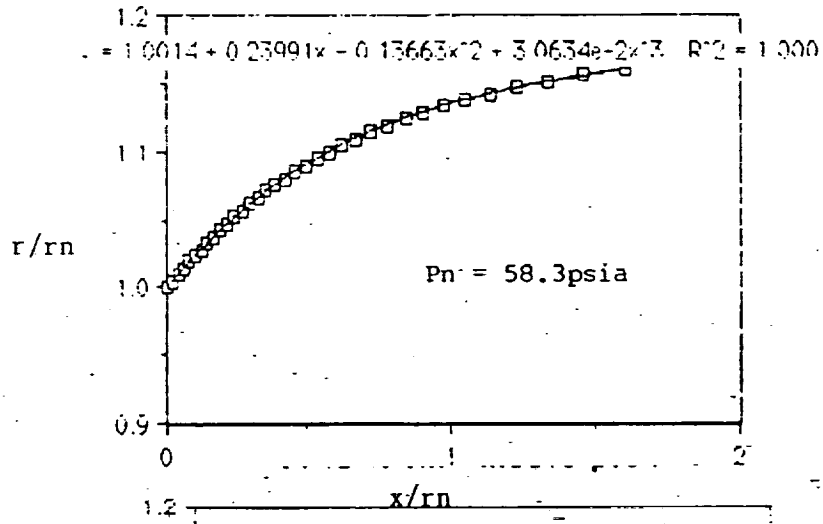
1.2
= 1.0014 + 0.23991x - 0.13663x^2 + 3.0634e-2x^3 R^2 = 1.000
1.1
1.0
0.9
r/rn
Pn = 58.3psia
0
2
x/rn

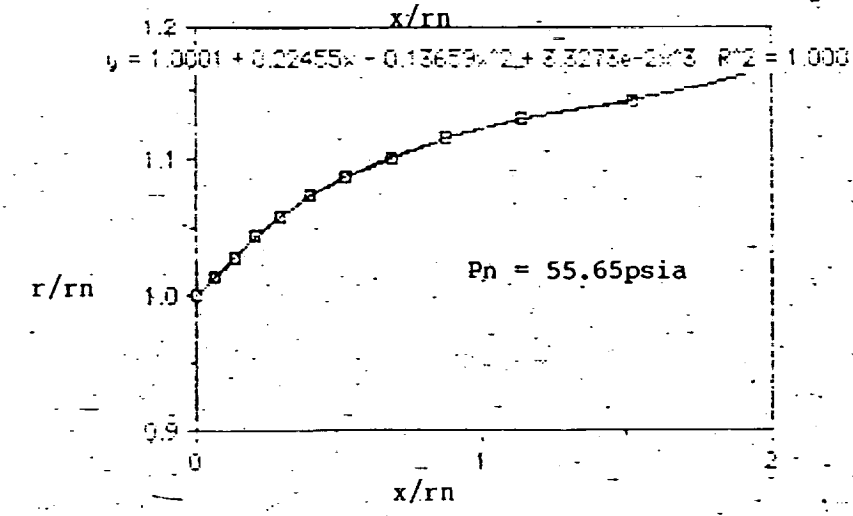
1.2
y = 1.0001 + 0.22455x - 0.13653x^2 + 3.3273e-2x^3 R^2 = 1.000
1.1
1.0
0.9
r/rn
Pn = 55.65psia
0
1
2
x/rn

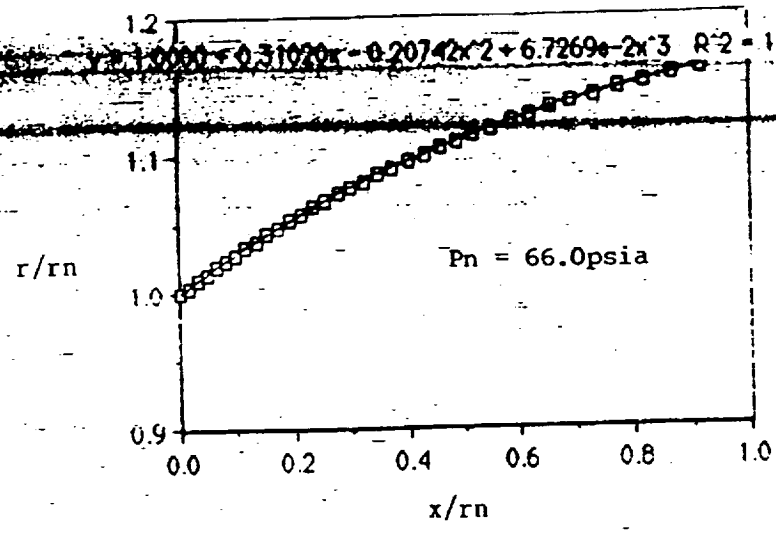

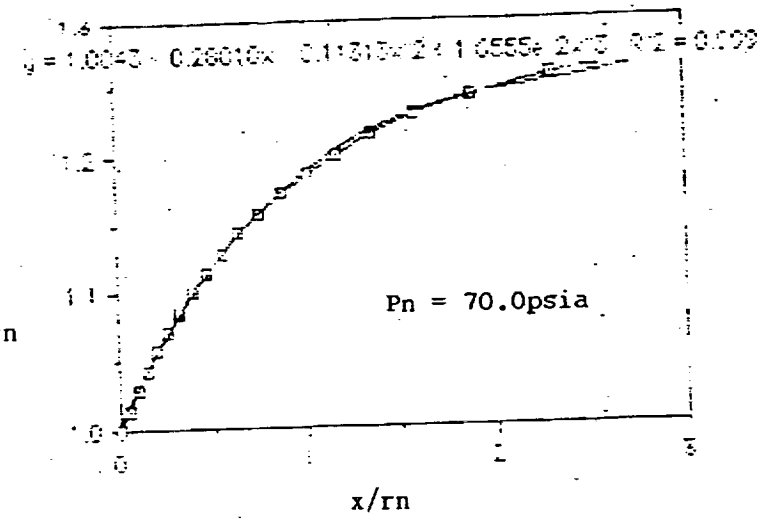

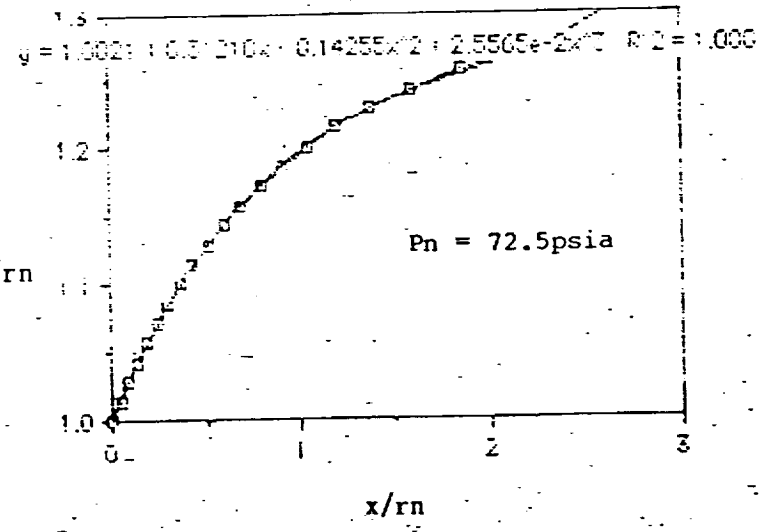

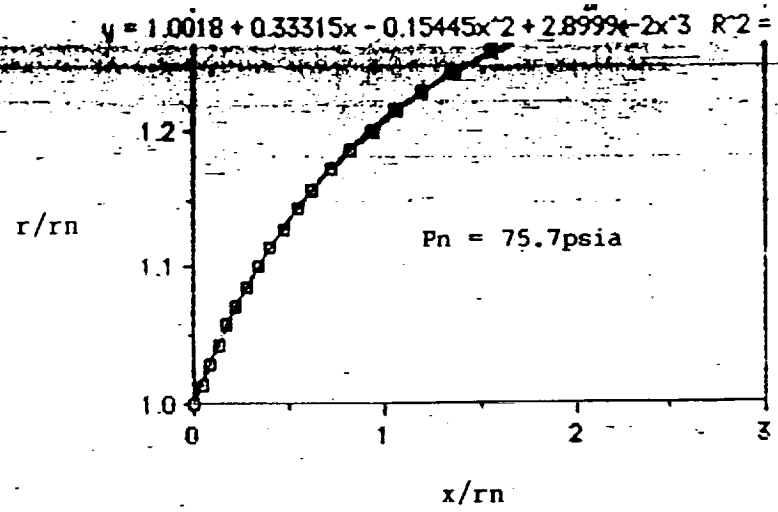

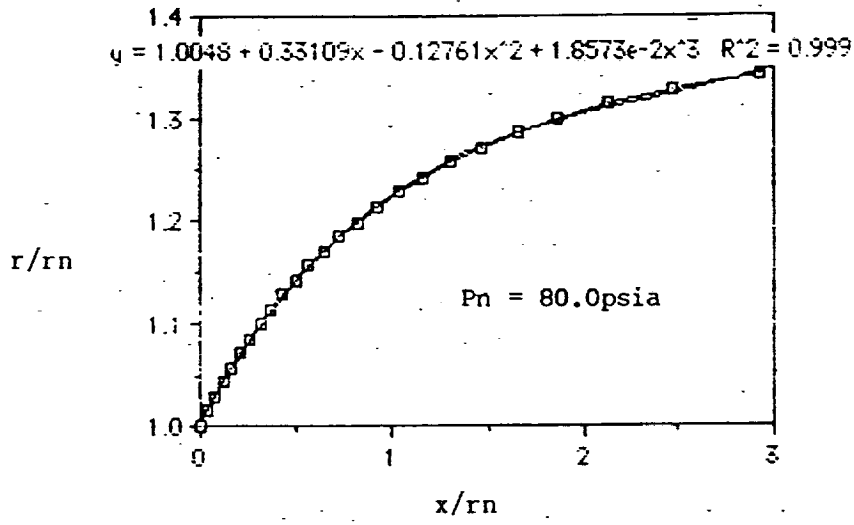

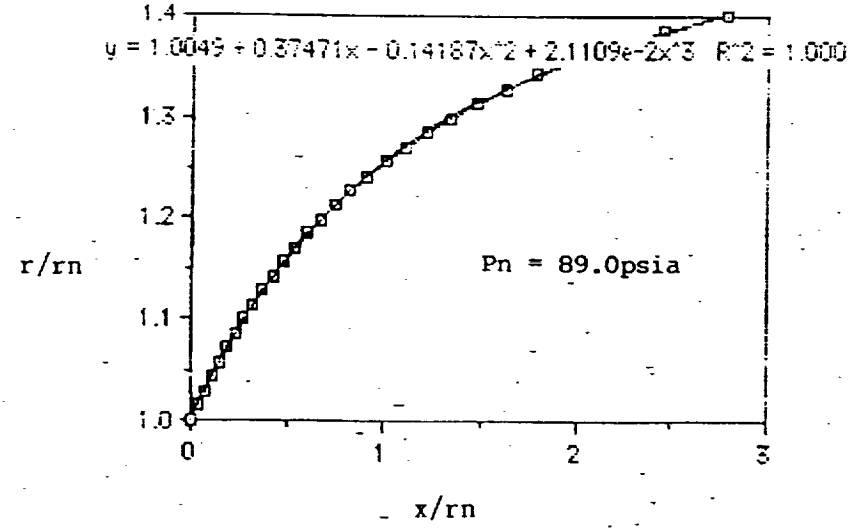

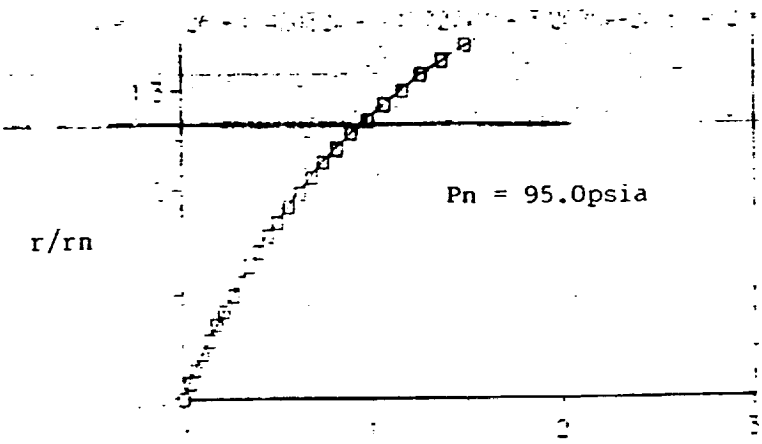

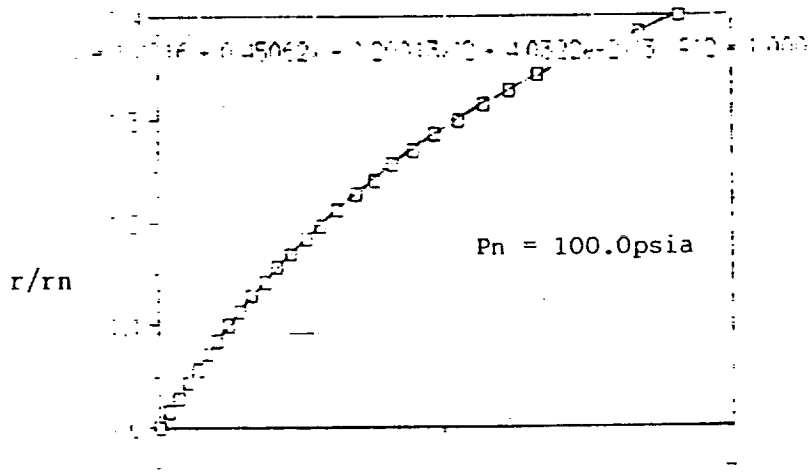

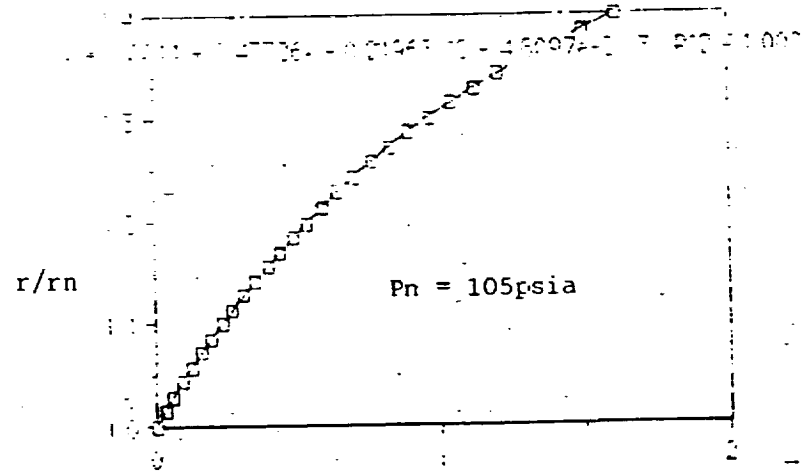

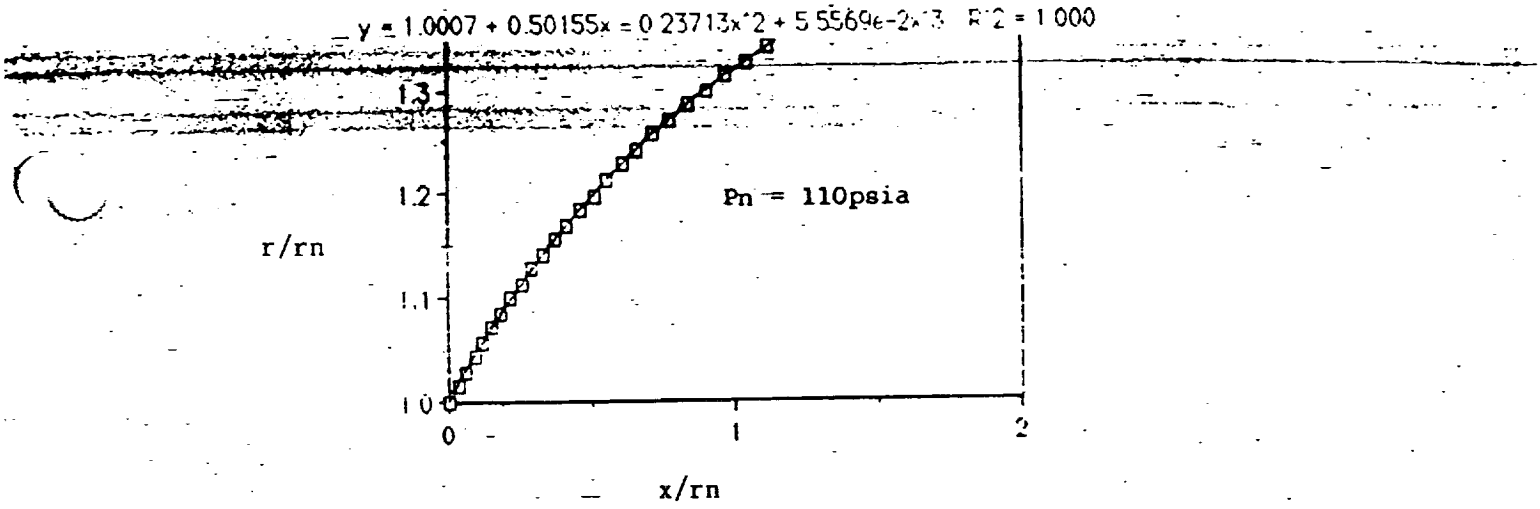

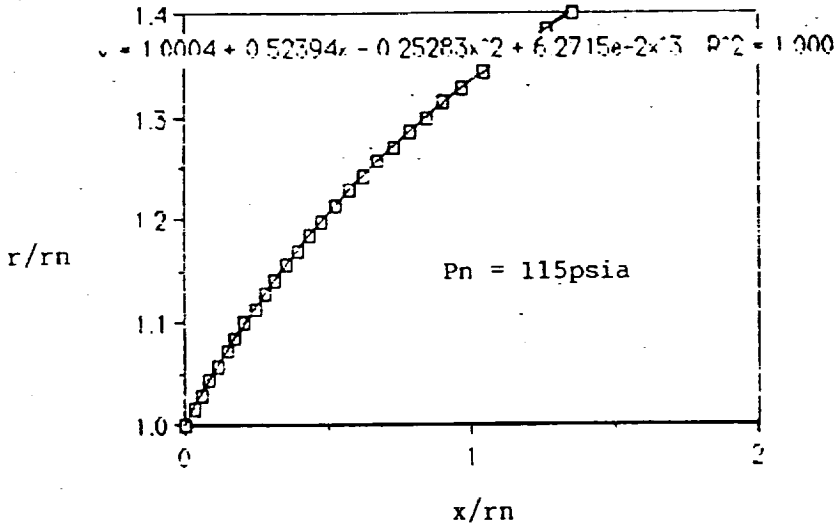

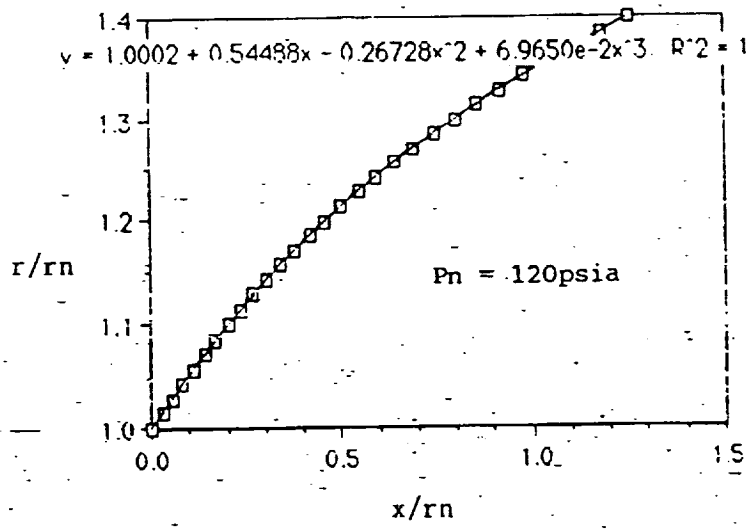

Appendix F

Jet Boundary Fortran Program

```
      PROGRAM PROG1
      INTEGER  I
      REAL   A,B(420),DR(420),    AST,ALF,TH,R,RR,AE,BRO,BRA,BRB,
     C       BRD,FRO,FRA,FRB,FRC,FRD,MRA,MRB,MRC,MRD,AA,MACH,
     C       CR(420),BA(420),DD,DF,PTJR,PTJ,BME,PJR,PJ,ME,BRC,H
      DATA   B/420*0.0/
      DATA   DR/420*0.0/
      DATA   CR/420*0.0/
      DATA   BA/420*0.0/
5     PRINT*,'   ENTER NOZZLE 'TOTAL PRESSURE' IN PSIA'
      PRINT*,'   ENTER 0.0 IF COMPLETED'
      READ*, PTJ
      IF(PTJ.EQ.0.0) THEN
        GOTO 300
      ENDIF
      H = 0.00108333
      PJ = PTJ*0.52828
      PJR = PJ/14.7
      PTJR = PTJ/14.7
      ME = SQRT(5.0*PTJR**0.285714-5.0)
      BME = SQRT(ME**2-1.0)
      ALF = 2.449489*ATAN(BME/2.449489) - ATAN(BME)
      AE = (1.0/ME)*(0.83333333+0.1666666*ME**2)**3
      R = 0.2275 + H
      FRO = 1.0/TAN(ALF)
      DR(1) = 1.0
      DD = 0.0
      DF = 0.0
      CR(1) = 0.2275
      BRO = SQRT(ME**2-1.0)
      PRINT*,'ASTE = ',AE
      PRINT*,'ME = ',ME
      DO 10          I=1,35
      RR = R/0.2275
      AST = (RR**2)*AE
      MRA = MACH(AST)
      BRA = SQRT(MRA**2-1.0)
      TH = 2.449489*(ATAN(BRA/2.449489)-ATAN(BRO/2.449489))-
     C       ATAN(BRA) + ATAN(BRO)
      FRA = 1.0/TAN(ALF-TH)
      R = R + H
      RR = R/0.2275
      AST = (RR**2)*AE
      MRB = MACH(AST)
      BRB = SQRT(MRB**2-1.0)
      TH = 2.449489*(ATAN(BRB/2.449489)-ATAN(BRO/2.449489))-
     C       ATAN(BRB) + ATAN(BRO)
      FRB =  1.0/TAN(ALF-TH)
      R = R + H
      RR = R/0.2275
      AST = (RR**2)*AE
      MRC = MACH(AST)
      BRC = SQRT(MRC**2-1.0)
      TH = 2.449489*(ATAN(BRC/2.449489)-ATAN(BRO/2.449489))-
     C       ATAN(BRC) + ATAN(BRO)
      FRC = 1.0/TAN(ALF-TH)
      A =   0.375*H*(FRO+3.0*FRA+3.0*FRB+FRC)
      AA = A/0.2275
      DR(I+1) = RR
      DD = DD + AA
      B(I+1) = DD
      CR(I+1) = R
      DF = DF + A
      BA(I+1) = DF
      FRO = FRB
      R = R + H
10    CONTINUE
```

```
      PRINT*,' NOZZLE TOTAL PRESSURE IS: ',PTJ
      PRINT*,' NOZZLE EXIT STATIC TO AMBIENT PRESSURE RATIO: ',PJR
      PRINT*,' ALF(RAD) = ',ALF
      PRINT*,'H = ',H
      PRINT*
        PRINT*,'              SOLUTION FOR JET BOUNDARY'
        PRINT*,'  R              R/RN              X              X/RN'
      DO 20     I=1,36
        PRINT21, CR(I),DR(I),BA(I),B(I)
21      FORMAT(1X,F6.4,3X,F12.8,3X,F12.8,3X,F12.8)
20    CONTINUE
      GOTO 5
300   END
      REAL FUNCTION MACH(X)
      REAL  MU,ML,MA,FMU,FML,FMA,X
        ML = 1.0
100     FML = (1.0/ML)*(0.8333333+0.1666666*ML**2)**3 - X
        MU = ML + 0.25
        FMU = (1.0/MU)*(0.8333333+0.1666666*MU**2)**3 - X
        FMV = FMU*FML
      IF(FMV.GT.0.0) THEN
        ML = MU
        GOTO 100
      ENDIF
200     MA = (MU-ML)/2.0 + ML
        FMA = (1.0/MA)*(0.8333333+0.1666666*MA**2)**3 - X
        FMV = FML*FMA
      IF(ABS(FMA).LT.0.1E-4) THEN
        MACH = MA
        RETURN
      ELSEIF(FMV.LT.0.0) THEN
        MU = MA
        FMU = (1.0/MU)*(0.8333333+0.1666666*MU**2)**3 - X
        GOTO 200
      ELSEIF(FMV.GT.0.0) THEN
        ML = MA
        FML = (1.0/ML)*(0.8333333+0.1666666*ML**2)**3 - X
        GOTO 200
      ENDIF
      END
```

END OF FILE REACHED - PRESS RETURN

Appendix G

Jet Structure Fortran Program

PROGRAM 2

```
      PROGRAM PROG5
      REAL      PTJ,PTJR,PJ,MA,MUW,BME,DEL,ALF,XA,NU,ML,MU,FML,FMU,
     C          FMV,MB,FMB,MUB,MUAV,FXL,XL,XU,EX,FXA,FXV,FXU,EBC,PB,
     C          RRN,A,B,C,D,XC,DELB,BET,MD,XD,MUA,BMU,BMB,EL,EA,EU,
     C          FEA,FEU,FEV,FEL,ECD,FXCV,FXCU,FXCL,FXC,XRN,BML,EM,XE,
     C          FXE,RRNA,EMAX,DMAX,PE,ME,DN,DD,DB,TD,TN,DIN,MF,DF,PF,
     C          MDOT,XZ,RRNB,RB,DRA,PD,EDE,TE,TB,TF,XY,DE,DELD,PJR,WRJ,
     C          PERC,ERR,RD,XX,RRND,XV,LD,RF,RH,RDN,LDN,BETA,CA,CB,CC,
     C          RDA,AA,RE,AFG,AFC,AE,MDOTA,MDOTB,XQ,RZ,ABC,AF,RHS,LHS,
     C          BETB,RDB,AB
50    PRINT*,'ENTER NOZZLE TOTAL PRESSURE IN PSIA'
      PRINT*,'ENTER 0.0 IF COMPLETED'
      READ*, PTJ
      IF(PTJ.EQ.0.0) THEN
         GOTO 950
      ENDIF
      PRINT*,'ENTER NOZZLE TOTAL TEMPERATURE IN DEG. RANKINE'
      READ*,TN
      PRINT*,'ENTER COEFFICIENT A'
      READ*,A
      PRINT*,'ENTER COEFFICIENT B'
      READ*,B
      PRINT*,'ENTER COEFFICIENT C'
      READ*,C
      PRINT*,'ENTER COEFFICIENT D'
      READ*,D
      PJ = PTJ*0.52828
      PJR = PJ/14.7
      PTJR = PTJ/14.7
      MA = SQRT(5.0*PTJR**0.285714-5.0)
      MU = ATAN(1.0/((MA**2.0-1.0)**0.5))
      BME = SQRT(MA**2.0-1.0)
      DEL = 2.449489*ATAN(BME/2.449489)-ATAN(BML)
      ALF = (1.570796+MU DEL)/2.0
      XA = 1.0/TAN(ALF)
      MUW = ATAN((MA**2.0-1.0)**(-0.5))
      MUA = MUW + DEL
      PRINT*,'MA = ',MA
      PRINT*,'DEL = ',DEL
      PRINT*,'ALF = ',ALF
      PRINT*,'XA =  ',XA
      PRINT*,'MUW = ',MUW
      PRINT*,'MUA = ',MUA
      NU = 2.0*DEL
      ML = 1.0
100   BML = SQRT(ML**2.0-1.0)
      FML = 2.449489*ATAN(BML/2.449489)-ATAN(BML)-NU
      MU = ML + 0.25
      BMU = SQRT(MU**2.0-1.0)
      FMU = 2.449489*ATAN(BMU/2.449489)-ATAN(BMU)-NU
      FMV = FMU*FML
      IF(FMV.GT.0.0) THEN
      ML = MU
      GOTO 100
      ENDIF
200   MB = (MU+ML)/2.0
      BMB = SQRT(MB**2.0-1.0)
      FMB = 2.449489*ATAN(BMB/2.449489)-ATAN(BMB)-NU
      FMV = FML*FMB
      IF(ABS(FMB).LT.0.1E-4) THEN
      PRINT*,'MB = ',MB
      GOTO 300
      ELSEIF(FMV.LT.0.0) THEN
      MU = MB
      GOTO 200
      ELSEIF(FMV.GT.0.0) THEN
      ML = MB
      BML = SQRT(ML**2.0-1.0)
      FML = 2.449489*ATAN(BML/2.449489)-ATAN(BML)-NU
      GOTO 200
      ENDIF
```

```
      PRINT*,'MUB = ',MUB
      PRINT*,'MUAV = ',MUAV
      XL = 0.0
400   FXL = A-TAN(MUAV)*(XL-XA)+B*XL+C*XL**2.0+D*XL**3.0
      XU = XL + 0.25
      FXU = A-TAN(MUAV)*(XU-XA)+B*XU+C*XU**2.0+D*XU**3.0
      FXV = FXU*FXL
      IF(FXV.GT.0.0) THEN
      XL = XU
      GOTO 400
      ENDIF
500   XD = (XU+XL)/2.0
      FXD = A-TAN(MUAV)*(XD-XA)+B*XD+C*XD**2.0+D*XD**3.0
      FXV = FXD*FXL
      IF(ABS(FXD).LT.0.1E-4) THEN
      PRINT*,'XD = ',XD
      GOTO 600
      ELSEIF(FXV.LT.0.0) THEN
      XU = XD
      GOTO 500
      ELSEIF(FXV.GT.0.0) THEN
      XL = XD
      FXL = A-TAN(MUAV)*(XL-XA)+B*XL+C*XL**2.0+D*XL**3.0
      GOTO 500
      ENDIF
600   PB = PTJ*(1.0+0.2*MB**2.0)**(-3.5)
      EBC=ASIN((((14.7/PB)+0.1666666)*(1.0/(1.1666666*MB**2.0)))**0.5)
      PRINT*,'EBC = ',EBC
      PRINT*,'PB = ',PB
      RRN = A+B*XD+C*XD**2.0+D*XD**3.0
      XC = RRN/TAN(EBC)
      PRINT*,'RRN =',RRN
      PRINT*,'XC = ',XC
      DELB = ATAN(((1.2*MB**2.0/(MB**2.0*(SIN(EBC))**2.0-1.0)-1.0)*
     C       TAN(EBC))**(-1.0))
      BET = EBC - DELB
      PRINT*,'DELB =',DELB
      PRINT*,'BET = ',BET
      MD = ((TAN(EBC)/(0.8333333*TAN(BET))-0.2)*(SIN(BET))**2.0)
     C     **(-0.5)
      PRINT*,'MD =  ',MD
      PRINT*
      DN = ((1.7117)*PTJ)/TN
      DTN = DN*1.5774409
      DB = DTN/((1.0+0.2*MB**2.0)**2.5)
      MF = ((MB**2.0+5.0)/(7.0*MB**2.0-1.0))**0.5
      PF = PB*(1.1666666*MB**2.0-0.1666667)
      PE = PF
      DD = DB*(2.4*MB**2.0*(SIN(EBC))**2.0)/(2.0+0.4*MB**2.0*
     C     (SIN(EBC))**2.0)
      TD = 39.6917/DD
      DF = DB*(2.4*MB**2.0)/(2.0+0.4*MB**2.0)
      TF = (2.602519*PF)/DF
      MDOT =  (0.086525*PTJ)/(TN**0.5)
      PRINT*,'TN = ',TN
      PRINT*,'DN = ',DN
      PRINT*,'DB = ',DB
      PRINT*,'MF = ',MF
      PRINT*,'PF = ',PF
      PRINT*,'DD = ',DD
      PRINT*,'TD = ',TD
      PRINT*,'DF = ',DF
      PRINT*,'MDOT = ',MDOT
800   EM = ASIN(((1.0/(1.4*MD**2.0))*(0.6*MD**2.0-1.0+(2.44
     C     0.48*MD**2.0+0.36*MD**4.0)**0.5))**0.5)
      DRA = (2.4*MD**2.0*(SIN(EM))**2.0)/(2.0+0.4*MD**2.0*
     C      (SIN(EM))**2.0)
      DMAX = (DRA-1.0)/(2.0*(DRA**0.5))
      PRINT*,'EMAX=' ,EM
      PRINT*,'DRA = ',DRA
      PRINT*,'DMAX = ',DMAX
      IF(DELB.GT.DMAX) THEN
      PRINT*,'*****DMAX IS EXCEEDED*****'
      WRJ = 2.0*(1.52*((PJR)**0.437)-0.5)
      PRINT*,'PRANDTL WAVELENGTH (NASA) IS',WRJ
      ELSE
      PRINT*,'*****DMAX IS NOT EXCEEDED*****'
      WRJ = 2.0*(1.55*((PJR-1.0)**0.5))
      PRINT*,'PRANDTL WAVELENGTH (NASA) IS',WRJ
      ENDIF
```

```
      DE = (DD*2.4*MD**2.0*(SIN(EDE))**2.0)/(2.0+0.4*MD**2.0*
     C       (SIN(EDE))**2.0)
      DELD = ATAN((((1.2*MD**2.0)/(MD**2.0*(SIN(EDC))**2.0-1.0)
     C          -1.0)*TAN(EDE))**(-1.0))
      BET = EDC - DELD
      ME = ((TAN(EDE)/(0.8333333*TAN(BET))-0.2)*(SIN(BET))**2.0)
     C       **(-0.5)


      IF(DELB.GT.DMAX) THEN
      PRINT*
      RH = 1.0/TAN(EBC) + 1.0/TAN(BET)
      RF = (1.0/RH)*(WRJ-XD)
      PRINT*,'RF = ',RF
      PRINT*,'RH = ',RH

      TE = (2.70012*PE)/DE
      TB = (2.70012*PB)/DB
      TF = (2.70012*PF)/DF


      RD = RRN - RF
      XX = RF/TAN(EBC)
      XZ = RF/TAN(BET)
      LD = XD  + XX
      XRN = XD + XX + XZ
      LDN = 0.055038+1.396*PJR-0.1978*(PJR**2.0)+0.01314*(PJR**3.0)
      RDN = -0.94807+0.67296*PJR-0.08638*(PJR**2.0)+0.004326*
     C        (PJR**3.0)

     LHS=(DB*MB*49.032*(TB**0.5)*3.14159265*((RRN*0.2275)**2.0))/144.
      RZ = (TAN(EBC))*XX
      RDB = RRN - RZ
      AB  =  3.14159264*((RRN*0.2275)**2.0)
     C       3.14159264*((RDB*0.2275)**2.0)
      ABC = AB/(SIN(EBC))
      AF = 3.14159264*((RDB*0.2275)**2.0)
      BETB= EDC - DELB
      RHS = (DD*MD*49.032*(TD**0.5)*(SIN(BETB))*ABC)/144.0
     C       +(DF*MF*49.032*(TF**0.5)*AF)/144.0


      PRINT*,'XX = ',XX
      PRINT*,'XZ = ',XZ
      PRINT*,'DISTANCE TO MACH DISC IS: ',LD
      PRINT*,'DISTANCE TO MACH DISC(NASA) IS: ',LDN
      PRINT*,'MACH DISC RADIUS IS: ',RD
      PRINT*,'MACH DISC RADIUS(NASA) IS: ',RDN
      PRINT*,'CALCULATED PRANDTL PRIMARY WAVELENGTH IS: ',XRN
      PERC = (LDN/LD)*100.0
      PRINT*,'PERC (LD) = ',PERC
      PRINT*,'WRJ = ',WRJ
      PRINT*,'XRN = ',XRN
      ERR = ABS(100.0-PERC)
      PRINT*,'PERCENT DEVIATION OF MACH DISC DISTANCE FROM NASA: ',ER
      PERC = (RD/RDN)*100.0
      PRINT*,'PERC (RD) = ',PERC
      ERR = ABS(100.0-PERC)
      PRINT*,'PERCENT DEVIATION OF MACH DISC RADIUS FROM NASA: ',ERR
      PRINT*
      PRINT*,'LHS = ',LHS
      PRINT*,'RHS = ',RHS
      PRINT*,'RZ = ',RZ
      PRINT*,'AB  = ',AB
      PRINT*,'RDB = ',RDB
      PRINT*,'ABC = ',ABC
      PRINT*,'AF = ',AF
      ENDIF
      PRINT*,'BET2 = ',BET
      PRINT*,'ME = ',ME
      PRINT*,'TE = ',TE
      PRINT*,'TB = ',TB
      PRINT*,'TF = ',TF
      IF(DELB.GT.DMAX) THEN
      GOTO 60
      ENDIF
      RRNB = A+B*(XD-XC)+C*(XD-XC)**2.0+D*(XD-XC)**3.0
      XE = RRNB/TAN(EDE)
      XRN = XD + XC + XE
      PRINT*,'RRNB = ',RRNB
      PRINT*,'XE = ',XE
      PRINT*,'CALCULATED PRANDTL WAVELENGTH IS ',XRN
      PERC =(WRJ/XRN)*100.0
```

PROGRAM 3

```
      PROGRAM PROG10
      REAL   MU,ML,FML,FMU,MA,FMA,FMV,MT,P,PI,TI,DT,PTN,TN,EF,
     C       PI,DI,TI,CD,AT,FZ,MDOT,MDOTI,CDA,FZA,EFA,FI,CF,AN
     C       PTR,CFA,CFB,ISP,FZC,FZF,FAC,MDOTA,MD,MDA,ISPI,ISPA,
     C       PSI,R,CFI
5     PRINT*,'ENTER NOZZLE TOTAL PRESSURE IN PSIA: '
      READ*,PTN
      IF(PTN.EQ.0.0) THEN
      GOTO 400
      ENDIF
      PRINT*,'ENTER NOZZLE TOTAL TEMPERATURE IN DEG R'
      READ*,TN
      PRINT*,'ENTER MEASURED THRUST IN LBF'
      READ*,FZ
      EF = 0.90
10    ML = 0.1
100   FML = (ML**4.0)*(EF-1.0)+(ML**2.0)*(EF*7.5-20.0)+12.5*EF
      MU = ML + 0.05
      FMU = (MU**4.0)*(EF-1.0)+(MU**2.0)*(EF*7.5-20.0)+12.5*EF
      FMV = FML*FMU
      IF(FMV.GT.0.0) THEN
      ML = MU
      GOTO 100
      ENDIF
200   MA = (MU+ML)/2.0
      FMA = (MA**4.0)*(EF-1.0)+(MA**2.0)*(EF*7.5-20.0)+12.5*EF
      FMV = FMA*FML
      IF(ABS(FMA).LT.0.1E-4) THEN
      MT = MA
      ELSEIF(FMV.LT.0.0) THEN
      MU = MA
      GOTO 200
      ELSEIF(FMV.GT.0.0) THEN
      ML = MA
      FML = (ML**4.0)*(EF-1.0)+(ML**2.0)*(EF*7.5-20.0)+12.5*EF
      GOTO 200
      ENDIF
      AN = 0.162597
      P = (0.2*MT**2.0)/(EF*(1.0+0.2*MT**2.0))
      PT = PTN*((1.0-P)**3.5)
      TT = TN/(1.0+0.2*MT**2.0)
      DT = (PT/TT)*2.700118
      PI = 0.52828*PTN
      TI = 0.8333333*TN
      DI = (PI/TI)*2.700118
      VT = MT*49.032*(TT**0.5)
      VI = 49.032*(TI**0.5)
      AT = FZ/(1.4*PI+PI-14.7)
      PTR = PTN/14.7
      CDA= (DT*VT)/(DI*VI)
      MDOT = 0.5320631*PTN*AT/(TN**0.5)
      MDOTA = DT*VT*AN/144.0
      MDOTB = (FZ-(PI-14.7)*AT*32.2)/VI
      MDOTI = 0.5320631*PTN*AN/(TN**0.5)
      MD = DI*VI
      MDA = DT*VT
```

```
      CD  = MDOT/MDOTI
      FAC = PT*MT*AN*(0.91939)/(TT**0.5) - MDOT
      IF(MDOTA.LT.MDOT) THEN
      EF = EF + 0.001
      GOTO 10
      ENDIF

      FI =(MDOT*VI)/32.2  + (PI-14.7)*AT
      FZC = MDOT*VI/32.2 + (PI-14.7)*AT
      R = PT/PTN
      PSI = (1.0+0.2*MT**2.0)**0.5
      CF  = FZ/(PTN*AN)
      CFA = (FZ*CD*0.5320631)/((TN**0.5)*MDOT)
      CFB = CD*0.81019*((5.0*EF*(1.0-R**0.2857143))**0.5)+
     C      (CD*0.5787*(R - 14.7/PTN))/(MT*R*PSI)
      ISPI = FZ/MDOTI
      ISPA = FZ/MDOT
      CFI = 1.2678745 - 14.7/PTN

300   PRINT*,'PTR = ',PTR
      PRINT*,'EF = ',EF
      PRINT*,'MT = ',MT
      PRINT*,'AT = ',AT
      PRINT*,'AN = ',AN
      PRINT*,'PTR = ',PTR
      PRINT*,'DT = ',DT
      PRINT*,'PT = ',PT
      PRINT*,'TT = ',TT
      PRINT*,'DI = ',DI
      PRINT*,'PI = ',PI
      PRINT*,'TI = ',TI
      PRINT*,'VT = ',VT
      PRINT*,'VI = ',VI
      PRINT*,'MDOT(ACT)= ',MDOT
      PRINT*,'MDOTA = ',MDOTA
      PRINT*,'MDOT(ISEN)= ',MDOTI
      PRINT*,'MD = ',MD
      PRINT*,'MDA = ',MDA
      PRINT*,'EFA = ',EFA
      PRINT*,'FZ = ',FZ
      PRINT*,'FI = ',FI
      PRINT*,'R = ',R
      PRINT*,'PSI = ',PSI
      PRINT*,'CD = ',CD
      PRINT*,'CDA = ',CDA
      PRINT*,'CFI = ',CFI
      PRINT*,'CF = ',CF
      PRINT*,'CFA = ',CFA
      PRINT*,'CFB = ',CFB
      PRINT*,'ISPI = ',ISPI
      PRINT*,'ISPA = ',ISPA


350   GOTO 5

400   END
END OF FILE REACHED - PRESS RETURN
```

Appendix H

NASA Graphical Data From Ref (3) and (13)

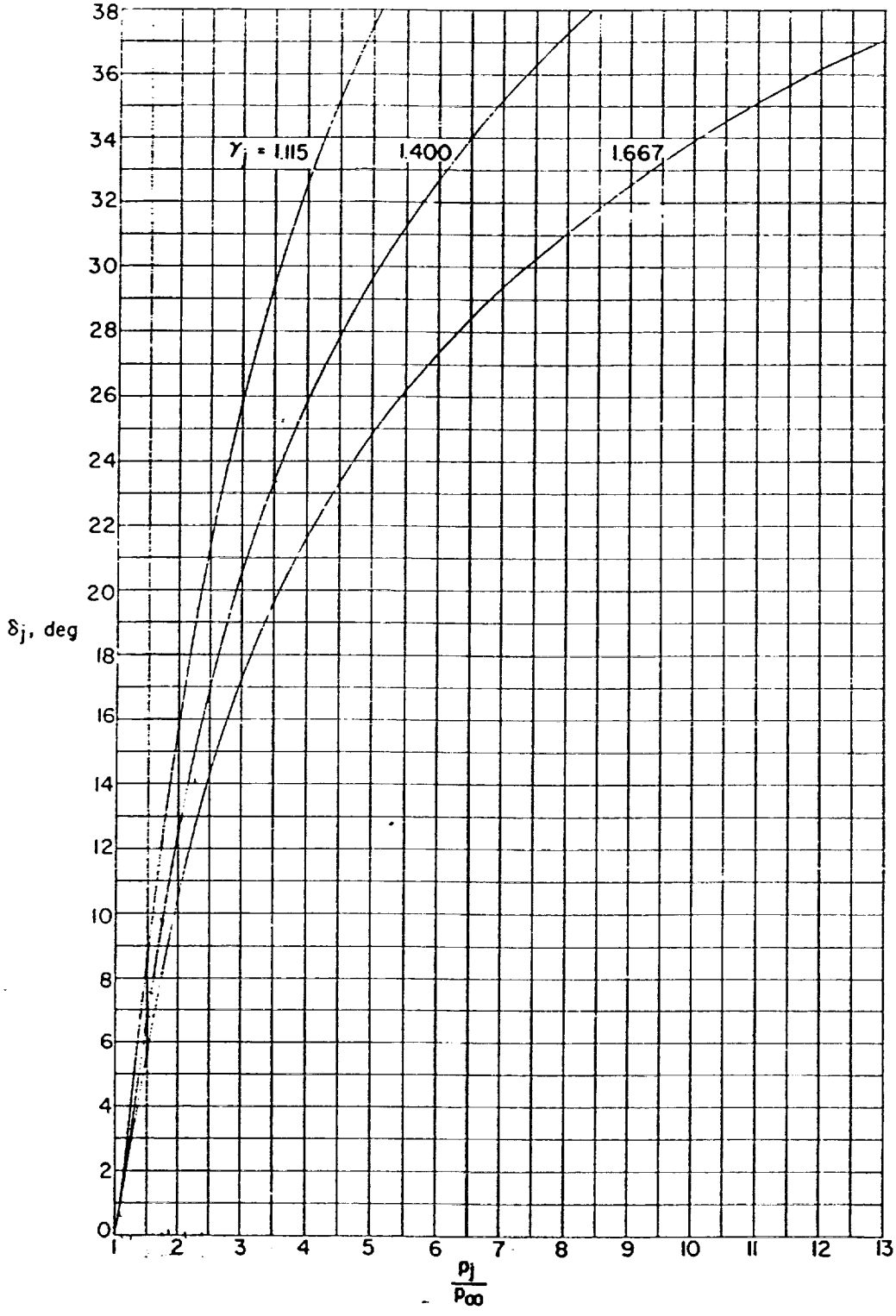

FIGURE 13.—Effect of the ratio of specific heats of the jet upon the initial inclination of the jet boundary. $M_j = 1.00$.

502683 O—59——7

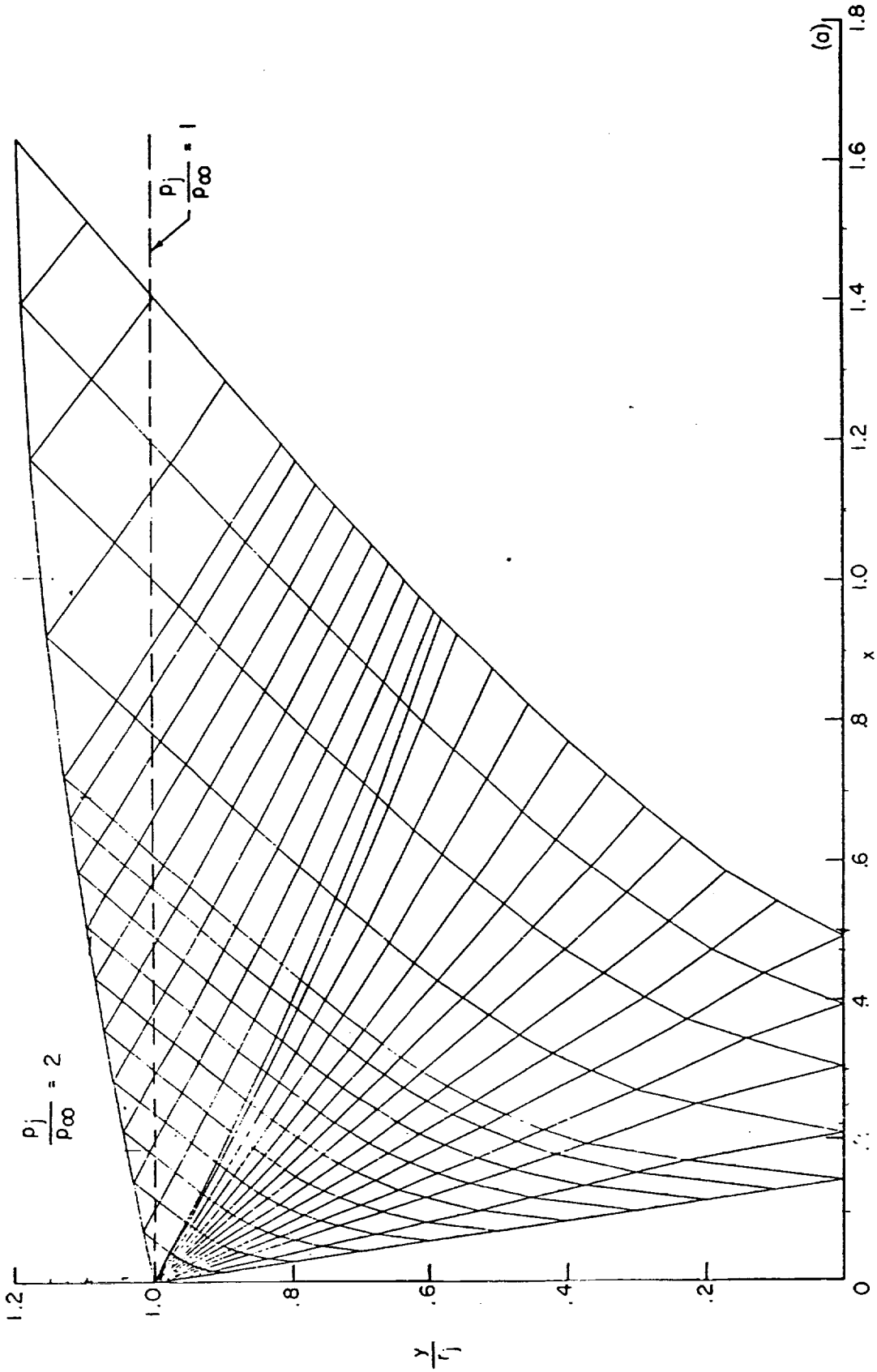

(a) $M_j = 1.01$; $\theta_N = 0°$; $\gamma_j = 1.400$.

FIGURE 14.—Characteristic nets.

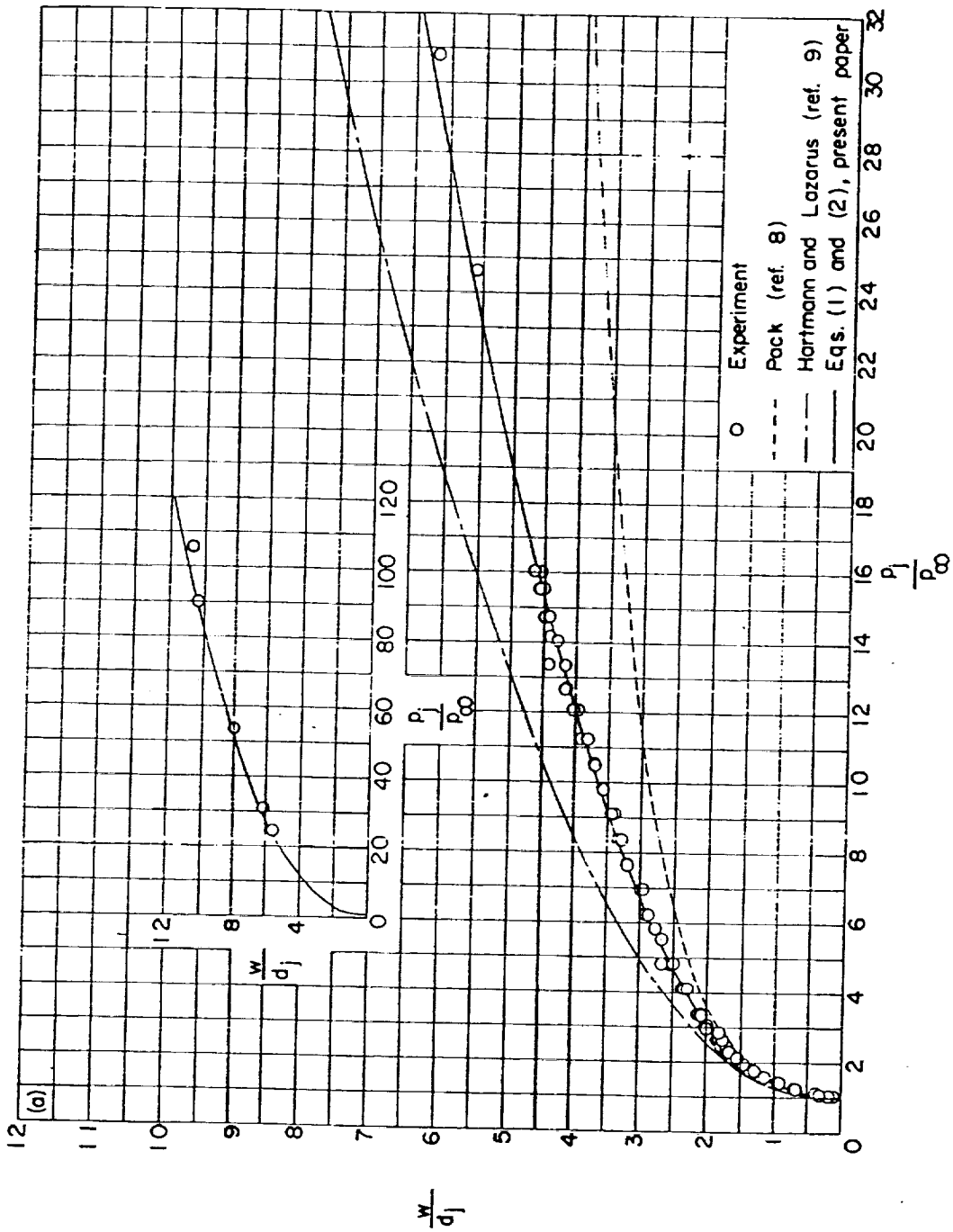

(a) $M_j = 1.00$.

FIGURE 7.—Effects of jet pressure ratio and nozzle divergence angle upon nondimensional primary wavelength.

502683 O—60——6

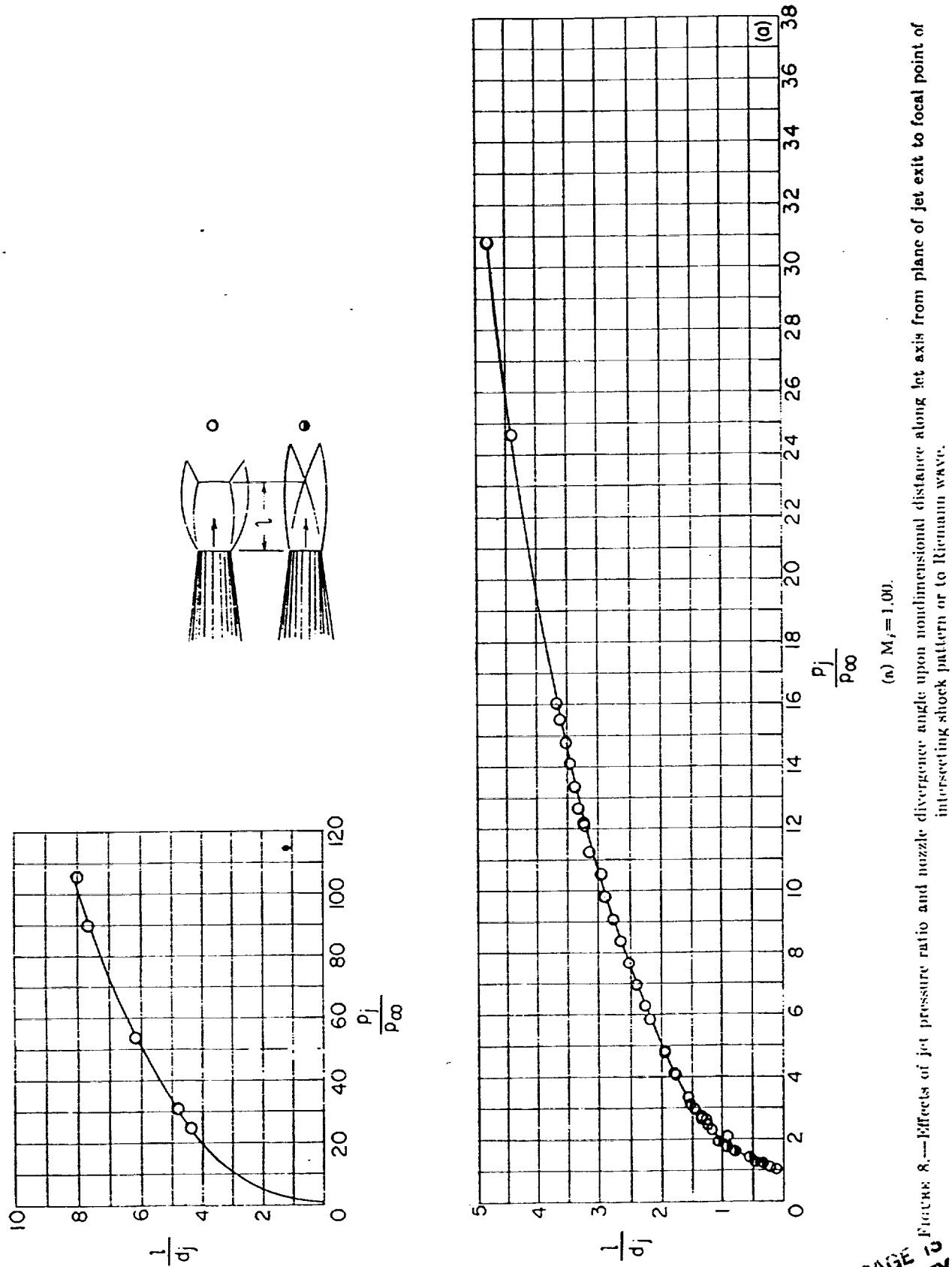

(a) $M_j = 1.00$.

FIGURE 8.—Effects of jet pressure ratio and nozzle divergence angle upon nondimensional distance along jet axis from plane of jet exit to focal point of intersecting shock pattern or to Riemann wave.

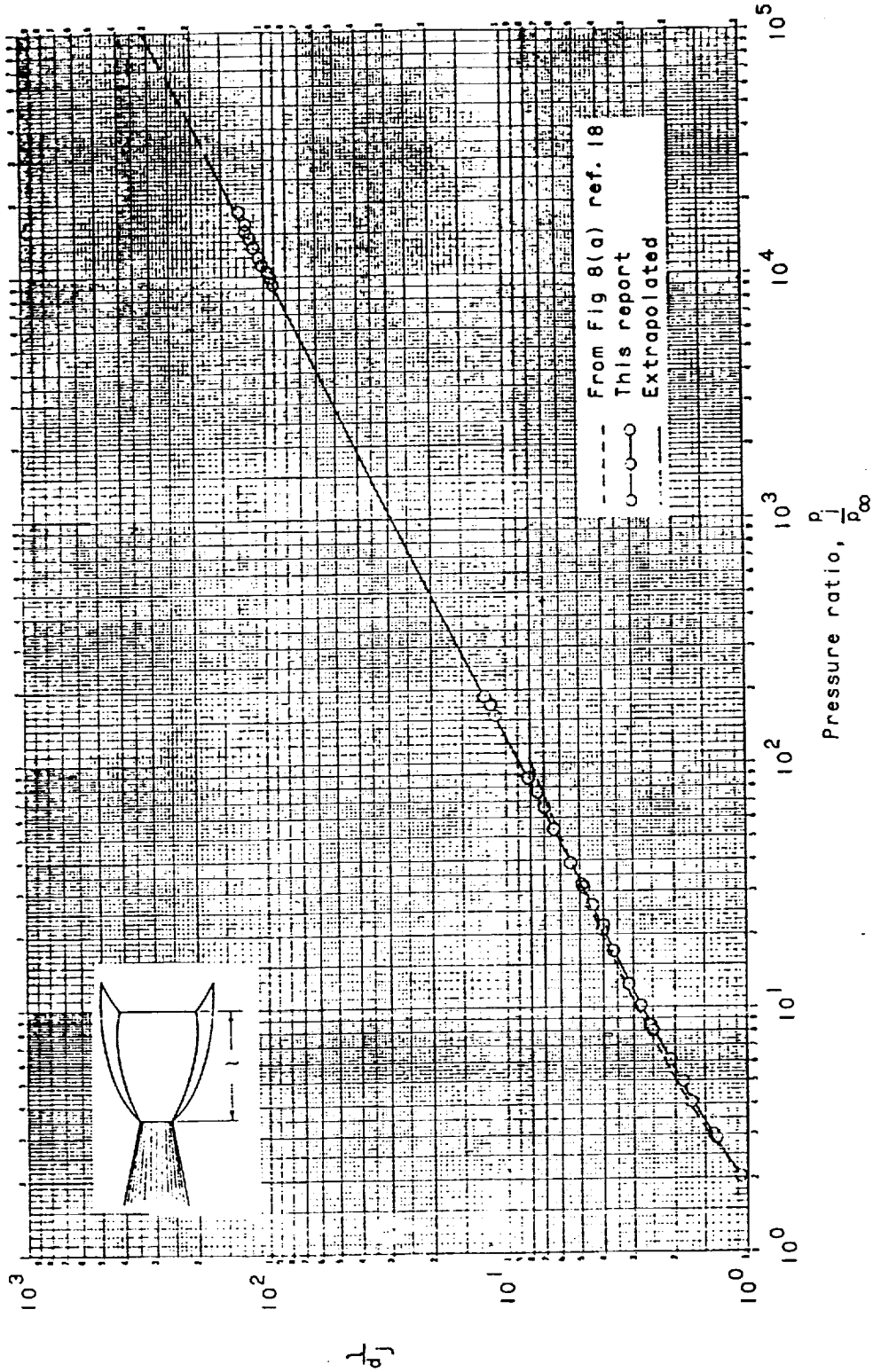

(a) $M_j = 1.0$; $\theta_N = 0^o$; $\gamma = 1.4$.

Figure 1[illegible]- Effect of jet pressure ratio upon nondimensional distance along jet axis from plane of nozzle exit to location of Riemann wave.

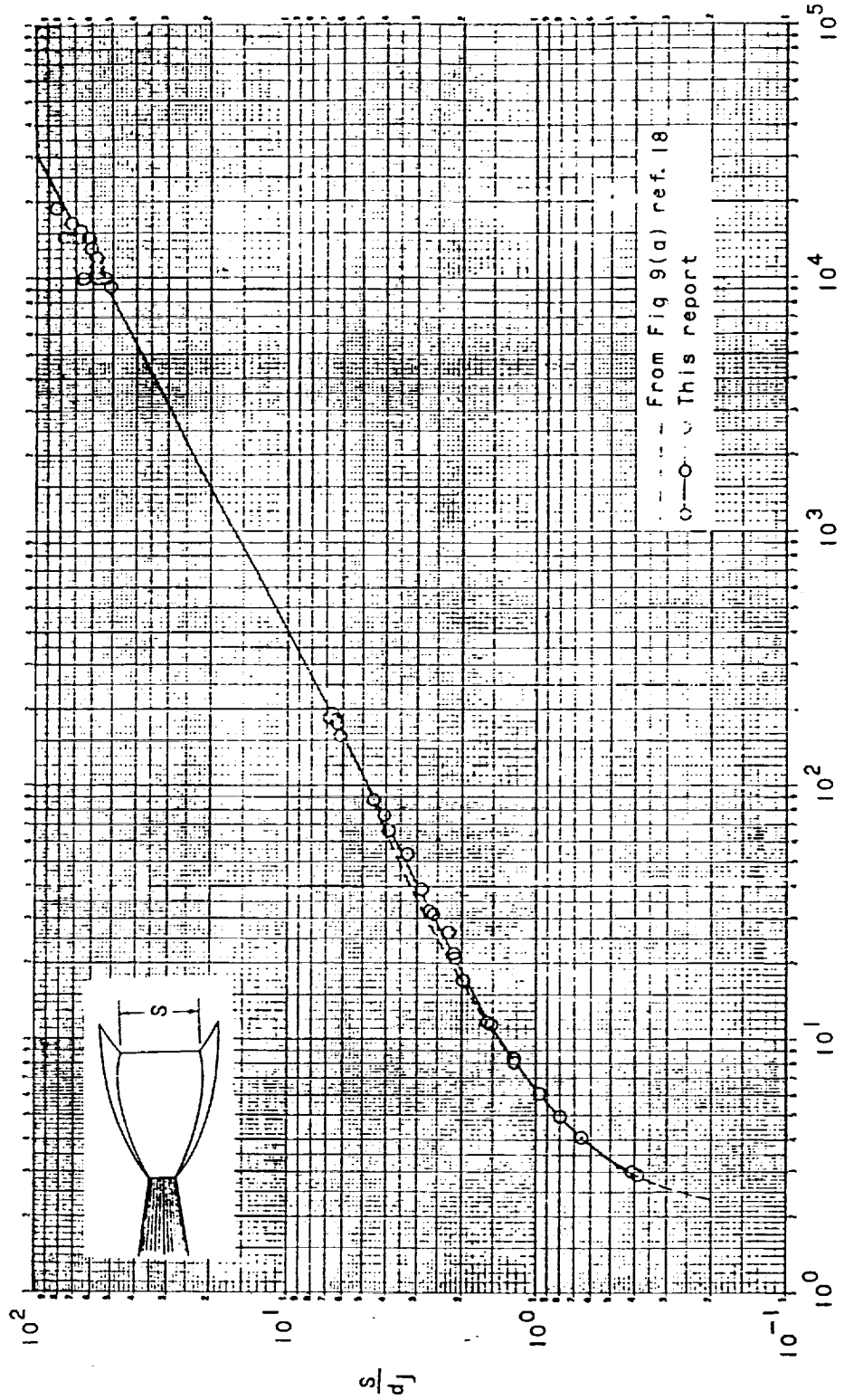

Figure 16.- Effect of jet pressure ratio upon nondimensional diameter of normal shock. $M_j = 1.0$; $\theta_N = 0°$; $\gamma = 1.4$.

Appendix I

Nozzle Geometry

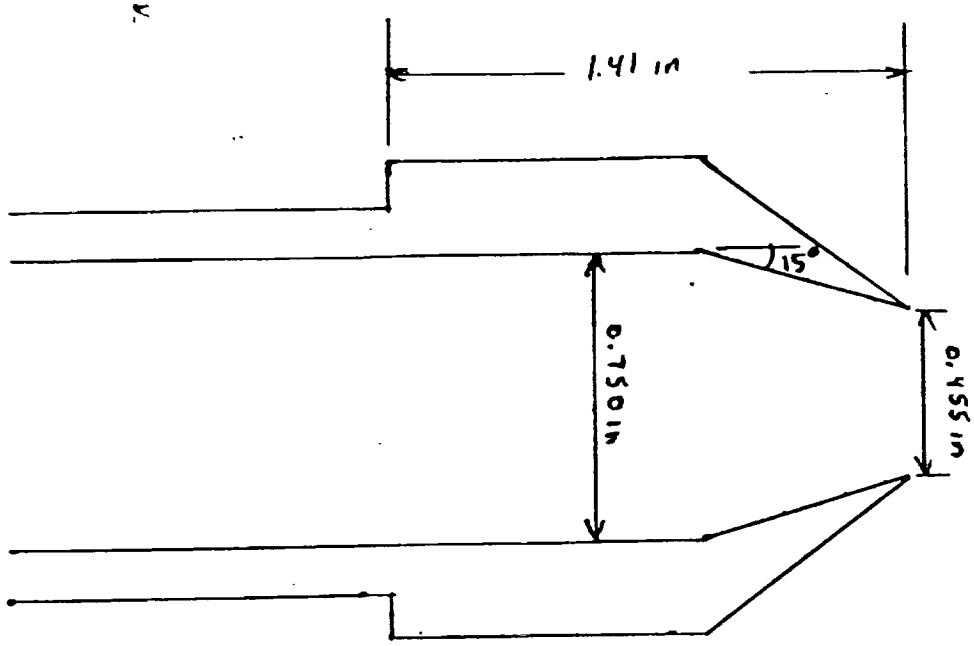

Straight Nozzle

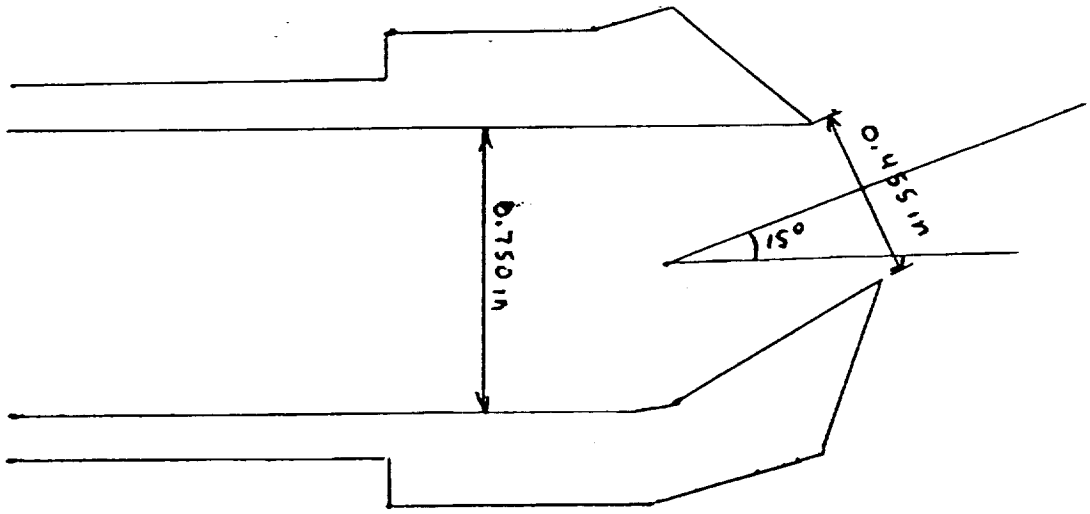

15 deg Nozzle

Appendix J

Thrust Stand Test Data

Straight Nozzle Data
12/19/1990

Pressure	Fx	Fy	Fz	Mx	My	Mz	R1	R2	R3	R4	R5	R6
psig	lb	lb	lb	in-lb	in-lb	in-lb	lb	lb	lb	lb	lb	lb
12.8	0.01	-1.80	2.88	-1.05	0.35	0.64	0.82	1.07	0.99	0.01	-0.98	-0.82
14.8	-0.02	-2.03	3.33	-0.67	0.22	0.60	1.02	1.18	1.13	-0.02	-1.09	-0.94
18	-0.05	-2.37	4.37	-1.55	0.43	0.68	1.25	1.61	1.51	-0.05	-1.27	-1.10
22.7	-0.01	-3.01	5.04	-1.20	0.35	0.84	1.52	1.80	1.72	-0.01	-1.61	-1.40
25.4	-0.02	-3.33	5.28	1.20	0.78	0.84	1.92	1.77	1.59	-0.02	-1.77	-1.56
24.5	-0.02	-3.15	5.52	0.75	0.26	0.84	1.94	1.82	1.76	-0.02	-1.68	-1.47
27.9	0.06	-3.58	6.27	0.98	0.91	0.88	2.22	2.13	1.92	0.06	-1.90	-1.68
29.7	-0.02	-3.85	6.55	1.03	0.56	0.84	2.32	2.18	2.05	-0.02	-2.03	-1.82
32.1	-0.01	-4.16	7.02	1.35	0.52	0.88	2.52	2.31	2.19	-0.01	-2.19	-1.97
32.1	-0.05	-4.14	7.06	1.25	0.35	0.96	2.52	2.31	2.23	-0.05	-2.19	-1.95
35.1	-0.03	-4.51	7.46	1.52	0.56	0.92	2.69	2.45	2.32	-0.03	-2.37	-2.14
39.8	-0.02	-5.16	8.31	2.40	0.35	0.96	3.09	2.65	2.57	-0.02	-2.70	-2.46
40.4	-0.09	-5.21	8.67	1.95	0.17	1.00	3.15	2.78	2.74	-0.09	-2.73	-2.48
41.2	0.02	-5.30	8.77	2.08	0.48	0.96	3.20	2.84	2.73	0.02	-2.77	-2.53
44.6	-0.04	-5.75	9.34	2.30	0.26	1.00	3.42	2.99	2.93	-0.04	-3.00	-2.75
50.7	-0.04	-6.57	10.52	2.80	0.26	1.00	3.88	3.35	3.29	-0.04	-3.41	-3.16
51.7	0.27	-6.70	10.67	3.10	0.87	0.88	3.97	3.45	3.25	0.27	-3.46	-3.24
56.4	-0.06	-7.34	11.78	3.10	0.00	1.12	4.34	3.72	3.72	-0.06	-3.81	-3.53
61.7	-0.08	-8.00	12.48	3.53	-0.22	0.88	4.63	3.90	3.95	-0.08	-4.11	-3.89
63.1	-0.11	-8.18	12.85	3.58	0.04	0.96	4.76	4.05	4.04	-0.11	-4.21	-3.97
66.2	-0.15	-8.58	13.33	3.80	-0.43	1.04	4.95	4.14	4.24	-0.15	-4.42	-4.16
78.7	-0.33	-10.33	15.60	4.65	-0.09	0.84	5.82	4.88	4.90	-0.33	-5.27	-5.06

System identification data

*** Chan.data ***

#	Name	Value	Unit
A	7*Pressure 1	29.2	psig
A	8*Pressure 2	37.3	psig
A	15*Press1	30.0	psig
A	16*Press2	38.3	psig
A	17*R1	19.48	lbf
A	18*R2	-17.49	lbf
A	19*R3	30.54	lbf
A	20*R4	5.15	lbf
A	21*R5	-1.13	lbf
A	22*R6	-1.94	lbf

***** 2-24-91

System identification data

*** Chan.data ***

#	Name	Value	Unit
A	7*Pressure 1	34.3	psig
A	8*Pressure 2	43.7	psig
A	15*Press1	34.7	psig
A	16*Press2	44.0	psig
A	17*R1	19.71	lbf
A	18*R2	-17.74	lbf
A	19*R3	31.31	lbf
A	20*R4	5.34	lbf
A	21*R5	-1.48	lbf
A	22*R6	-2.43	lbf

***** 2-24-91

System identification data

*** Chan.data ***

#	Name	Value	Unit
A	7*Pressure 1	40.6	psig
A	8*Pressure 2	51.2	psig
A	15*Press1	40.9	psig
A	16*Press2	51.6	psig
A	17*R1	20.07	lbf
A	18*R2	-17.94	lbf
A	19*R3	32.41	lbf
A	20*R4	5.64	lbf
A	21*R5	-1.95	lbf
A	22*R6	-3.03	lbf

***** 2-24-91

System identification data

*** Chan.data ***

#	Name	Value	Unit
A	7*Pressure 1	34.0	psi
A	8*Pressure 2	43.2	psi
A	15*Press1	34.0	psi
A	16*Press2	43.1	psi
A	17*R1	19.73	lb
A	18*R2	-17.68	lb
A	19*R3	31.18	lb
A	20*R4	5.33	lb
A	21*R5	-1.23	lb
A	22*R6	-2.15	lb

***** 2-24-91

System identification data

*** Chan.data ***

#	Name	Value	Unit
A	7*Pressure 1	41.0	psi
A	8*Pressure 2	51.5	psi
A	15*Press1	41.0	psi
A	16*Press2	51.5	psi
A	17*R1	20.12	lbf
A	18*R2	-17.98	lbf
A	19*R3	32.39	lbf
A	20*R4	5.63	lbf
A	21*R5	-1.72	lbf
A	22*R6	-2.80	lbf

***** 2-24-91

System identification data

*** Chan.data ***

#	Name	Value	Unit
A	7*Pressure 1	42.2	psi
A	8*Pressure 2	53.2	psi
A	15*Press1	42.0	psi
A	16*Press2	52.8	psi
A	17*R1	20.15	lbf
A	18*R2	-17.98	lbf
A	19*R3	32.55	lbf
A	20*R4	5.66	lbf
A	21*R5	-1.99	lbf
A	22*R6	-3.10	lbf

***** 2-24-91

System identification data